Distributed parameter model-based control of water activity and concentration of reactants in a polymer electrolyte membrane fuel cell

Maria Sarmiento-Carnevali[a,1,*], Maria Serra[a], Carles Batlle[b]

[a] *Institut de Robòtica i Informàtica Industrial (CSIC-UPC), C/ Llorens i Artigas 4-6, 08028 Barcelona, Spain*
[b] *Departament de Matemàtiques & IOC, Universitat Politècnica de Catalunya, EPSEVG, Av. V. Balaguer s/n, 08800 Vilanova i la Geltrú, Spain*

Abstract

Water management is still a key challenge for optimal performance and durability of polymer electrolyte membrane (PEM) fuel cells. Water levels along the channel in a PEM fuel cell present important spatial variations that should be taken into account to avoid both local flooding and local drying. In this work, a decentralised model predictive control scheme is designed to maintain the water activity on both anode and cathode sides of the PEM at appropriate levels. The proposed strategy tackles the accumulation of liquid water on the surface of the catalyst layers, and the possibility of local drying, by controlling observed water activity spatial profiles. Classic PEM fuel cell issues like reactant starvation are also considered. High control performance is achieved. The strategy is applied to a validated distributed parameter PEM fuel cell model. Results show increased cell power density in comparison to non-spatial control strategies.

Keywords: PEM fuel cell, water management, distributed parameter modeling, model predictive control, performance enhancement

*Corresponding author.
Email address: msarmiento@iri.upc.edu (Maria Sarmiento-Carnevali)
[1] *Telephone numbers:* +34 (93) 401 57 89; Fax: +34 (93) 401 57 50.

1. Introduction

In recent years, the PEM fuel cell technology has been incorporated to the R&D plans of many key companies in the automotive, stationary power and portable applications sectors [1, 2, 3]. However, despite recent developments, the technology is not mature enough to be significantly introduced into the energy market. Performance, durability and cost are the key challenges for PEM fuel cells.

The operation of a PEM fuel cell is fundamentally linked to the presence of water in the cell, therefore, water management is critical and one of the most widely studied issues in PEM fuel cell technology. Proper water management requires meeting two conflicting needs: (i) adequate membrane and catalyst layer hydration for high proton conductivity, and (ii) avoidance of excess water in the catalyst layers, gas diffusion layers and gas flow channels within the bipolar plates [4, 5]. Accumulation of condensed water inside the cell obstructs the flow of reactants through the gas channels and pores of the gas diffusion layer, and can also block access to the reaction sites in the catalyst layer. In the worst case scenario this condition leads to cell failure due to flooding.

Excess water blockages can instantly lead to reactant starvation and immediate drop in cell potential. Long cell exposure to fuel or oxidant starvation can cause severe degradation. It has been observed that, in the case of gross fuel starvation, cell voltages can become negative, as the anode is elevated to positive potentials, and the carbon is consumed given the lack of fuel. This means the anodic current will be provided by carbon corrosion to form carbon dioxide, which results in permanent damage to the anode catalyst layer. Similarly, during oxygen starvation the reaction at the cathode will produce hydrogen. The presence of fuel and oxidant on the wrong side of the membrane will also lead to reverse cell potential, carbon corrosion and subsequently to damaged components [4, 5].

Poor water management can also lead to a shortage of water resulting in membrane dehydration. This condition, more likely to occur at the anode side,

causes higher membrane protonic resistances and consequently a drop in cell voltage and overall cell power. Long-term operation of the membrane in a dried state can also result in increased generation of radicals that enhance membrane degradation [6, 7].

Water transport within a fuel cell has been studied through electrochemical impedance spectroscopy analysis or neutron imaging techniques, which generate important results and conclusions at cell research and development stages [8, 9, 10]. Some authors have covered the analysis of liquid water formation using transparent flow field single cells for direct experimental visualisation [11]. In addition, analyses of the effectiveness of various gas diffusion layer materials to remove water from the electrodes through the flow field have been published [12]. Another set of works focuses on improvement of flow field design to optimise water removal actions, including interdigitated flow field design [13, 14]. Certain techniques such as electro-osmotic pumping have also been considered [15].

One of the most important research efforts in the PEM fuel cell field corresponds to the incorporation of advanced control strategies to ensure, according to the power required, a proper dynamic response and operating conditions of the fuel cell that maximise efficiency and durability. Approaches available in the literature include linear and nonlinear controllers. Considerable progress has been made in order to avoid starvation and overheating of the fuel cell, regulate power output and manage temperature control [16, 17, 18, 19, 20, 21, 22, 23].

In the area of water management control, manipulation of the operating conditions is a very common strategy to mitigate flooding. These approaches include: increasing cathode gas flow rate well above stoichiometric levels to remove water through evaporation and advection [24, 25, 13], flushing the cathode periodically with momentarily high air flow rate (blowdown) [26, 13], increasing gas temperature [27], creating a coolant temperature gradient [28], and employing reactant gas counter-flow operation [29]. This class of strategies often cause significant parasitic losses, thermal stress and reduced system efficiency.

Several authors have demonstrated that variations in the concentrations of hydrogen, oxygen and water, as well as temperature and many other variables,

have significant effects on the performance and durability of PEM fuel cells. These variables exhibit internal spatial dependence in the direction of the fuel and oxygen streams of the anode and cathode. Highly non-uniform spatial distributions in PEM fuel cells result in local over-heating, cell flooding, accelerated ageing, and lower power output than expected [30, 31]. Model-based control strategies are normally considered to account for the internal behaviour of a PEM fuel cell [32], particularly in cases where direct measurements are not available. A distributed parameter model is necessary to analyse spatial profiles.

Despite several authors having demonstrated the importance of spatial variations of certain variables in PEM fuel cells, not many works available in the literature target the control of spatial profiles. Most model-based control designs use lumped-parameter models due to their simplicity and convenience for controller performance [16, 17, 18, 19]. Regarding the task of PEM fuel cell water management, model-based control strategy proposals available in the literature focus mainly on the cooling and humidification systems. The temperature of the cell and the amount of external humidification, if any, are the preferred parameters to control liquid water formation in the fuel cell [33, 34, 35, 36]. In general, these controllers rely on external measurable cell variables such as gas inlet and outlet relative humidity, cell temperature and cell current, neglecting internal humidification spatial profiles.

There are very few works that can be found in the literature regarding distributed parameter model-based control. Methekar et al. presented a dynamic analysis and linear control strategies for proton exchange membrane fuel cell using a distributed parameter model [37]. In this case, a linear ratio control strategy and a multi-input multi-output control strategy were presented. The control objectives were the average power density and the temperature of the solid. This work showed that, by choosing the proper manipulated variables, the PEM fuel cell did not exhibit sign change in gain and hence could be controlled by a linear controller. Both control strategies were able to deal with oxygen starvation. However, the control targets still did not exploit the capabilities of the model. Likewise, Chen et al. developed a 1D model that captures the

behaviour of water transport through the membrane [38]. In this work, water management control strategies were proposed considering a few model parameters, such as humidification coefficients, without considering spatial behaviour of water through the membrane as a controlled variable. Other control-oriented distributed parameter model proposals are available in the literature [39, 40]. Such models, however, have not been exploited within a control scheme or their computational complexity has not been analysed.

In recent years, a few studies on nonlinear control of PEM fuel cells have been conducted. Nonlinear controllers present several advantages for fuel cell systems, given the intrinsic nonlinearities of the system under study. Moreover, this kind of controller can guarantee stability of the closed-loop system over a wide range of operation conditions. Strategies such as nonlinear model predictive control, sliding mode control and passivity based control have been applied to fuel cell systems. Very few of these strategies have been designed for distributed parameter models due to increased controller complexity.

A sliding mode controller for the air supply system of a PEM fuel cell was developed by Garcia-Gabin et al. [41] on a medium size PEM fuel cell showing successful performance. The objective required a fast response of the control scheme in order to avoid oxygen starvation during load changes and this controller showed the ability to deal with load changes rapidly for all the operation range. The sliding mode structure gives the possibility of swiftly tracking different loads without increasing the computational effort.

Mangold et al. [42] published a contribution in the field of distributed parameter control. In this work a passive controller was presented that was able to keep the water content and the temperature of a PEM fuel cell on constant levels under changes of the electrical load. The controller was tested in simulations and compared with conventional linear control approaches such as a linear LQ optimal controller that was developed for comparison purposes. This controller was shown to be able to handle fast load changes. However, the control target was not clearly established to target PEM fuel cell challenges like flooding or proper membrane humidification.

The aim of this research paper is to implement and demonstrate a model-based control strategy that takes into account spatial profiles of internal cell variables by using an order-reduced distributed parameter model as a reference model. This reference model is linear with adaptive features. This condition allows the strategy to be stable in a desired range of operation whilst maintaining the reduced computational complexity of a linear model. This is an important advantage of the proposed control strategy over nonlinear approaches.

There is a trade-off between model computational complexity and model accuracy in the field of model-based control. As previously stated, using a distributed parameter model as reference model can lead to a high level of complexity in the controller. Therefore, the approach in this work is to design and implement a control strategy that achieves a balance between mentioned reference model conditions. This is accomplished with model order reduction techniques, which preserve input-output behaviour of the original full order validated model according to selected control targets. Such techniques aid in the derivation of simplified distributed parameter models that properly represent certain desired variables from spatial profiles. Moreover, the control strategy is applied to a validated full order non-linear distributed parameter model of a single PEM fuel cell, previously published in Sarmiento-Carnevali et al. [43].

Throughout the following sections, a decentralised water activity control strategy based on two distributed parameter model predictive controllers is designed and implemented. One of the controllers focuses on the anode side and the other focuses on the cathode side. The aim of the strategy is to monitor and control observed water spatial profiles on both sides of the membrane to appropriate levels. These target values are carefully chosen to combine proper membrane, catalyst layer and gas diffusion layer humidification, whilst the rate of accumulation of excess liquid water is reduced. The key objective of this approach is to decrease the frequency of water removal actions that cause disruption in the power supplied by the cell, increased parasitic losses and reduction of cell efficiency [5]. A variation of the water activity control strategy, which includes the control of spatial distribution of reactants in the fuel and air channels,

is also presented and analysed.

The paper is organised as follows. Section 2 introduces the PEM fuel cell model used. Section 3 describes in detail the proposed decentralised control scheme. Section 4 presents variations of the control strategy design that lead to improved approaches. Section 5 shows control results for different variables in challenging test scenarios for water management. In this section, the proposed spatial control scheme is compared to a traditional feed-forward inlet gas humidification strategy. The different variations of the control strategy are also analysed. Finally, Section 6 presents concluding remarks and on-going work.

2. Distributed parameter PEM fuel cell model

The system model under study is a single-channel single PEM fuel cell that consists of gas channels, gas diffusion layers, catalytic electrodes, the polymer electrolyte membrane and a liquid cooling system (end plates).

The phenomena inside the MEA that is modelled includes: gas diffusion through porous media, electrochemistry reactions, proton transport through proton-conductive polymer membrane, water transport through polymer membrane, including both electro-osmotic drag and back diffusion, electron conduction through electrically conductive cell components and thermal transport. Outside the MEA, the phenomena is described by models of mass and thermal transport. The single-channel model is considered a fine representation of an entire cell with several channels given the periodicity of the process. This model is built upon the following assumptions:

- Fluid in gas channels and in the gas diffusion layers behaves like an ideal gas.
- Gas channels possess storage capacity for mass and energy.
- No storage capacity for mass is considered for the gas diffusion layers and the catalyst layers.
- Pressure at the outlet of the gas channels is equal to ambient pressure.

- Liquid water formation in the catalyst layers is modelled through an empirical logic that estimates water coverage on the electrochemical surface area. This feature of the model is also used to consider mass transport losses due to liquid water formation.

- Electrical conductivity of the membrane depends on its water content. It is calculated using an empirical relation reported in [44].

- The MEA components, i. e. membrane, catalyst layers and gas diffusion layers, are on the same temperature level T.

- There are no gradients of electrical potential in the electrodes.

- The ohmic resistance of the cell is caused by the membrane.

- Activation losses are considered. Fuel and electrons crossover losses and concentration losses are neglected. However, the cell model will be operated in the ohmic region of the polarisation curve.

Figure 1 shows the structure of the cell under analysis. The model is nonlinear with dimension 1 + 1D, which considers transport through the MEA as a series of lumped parameter models, i.e. one single volume for each layer of the cell in the y-direction, coupled to 1D models in the direction of the gas flows, i.e. spatial gradients in the z-direction of each layer of the cell. The 1D direction has been discretised in n segments using the central finite differences approach. The variables of interest are also shown in the scheme.

This research work focuses on a single PEM fuel cell model because its simplicity facilitates the analysis and control of spatial variations of temperature, reactants concentration, water activity in the catalyst layers and gas diffusion layer or water content in the membrane, which are important variables related to fuel cell water management and corresponding degradation mechanisms.

Being spatial variations the focus of this research work, it was considered appropriate to develop a model that would clearly show the behaviour of these variables in one cell. This approach would allow the demonstration of feasibility,

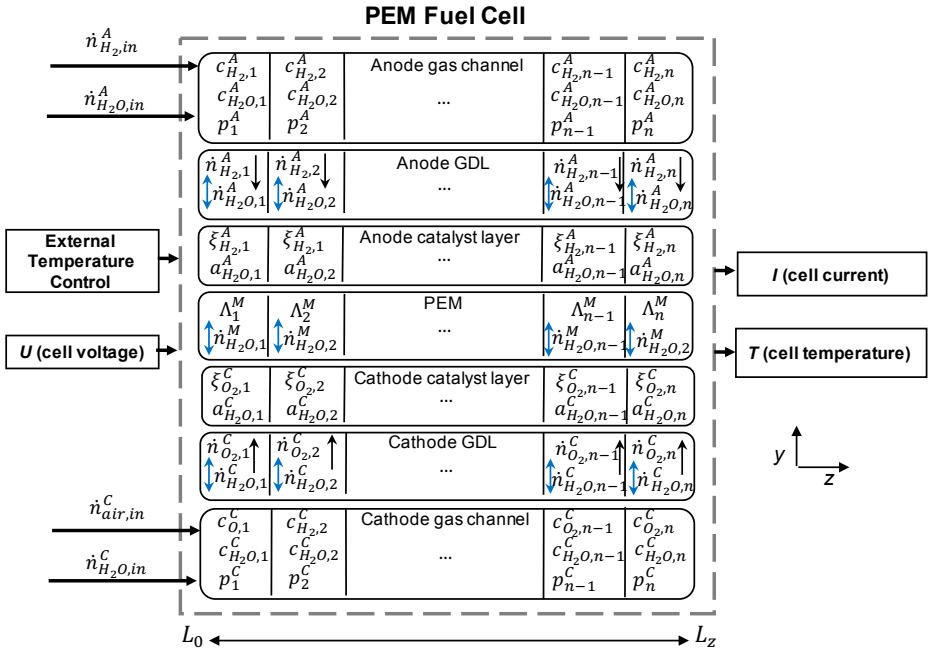

Figure 1: PEM fuel cell model scheme

reliability and performance of the proposed control strategy over spatial profiles as controlled variables.

Relevant discretised model equations for the different cell layers used in the control design stage are presented in the following sections. This distributed parameter model was designed, implemented and validated during a previous phase of this work. Extended model details can be found in [43]. Refer to Table 1 for nomenclature.

2.1. Gas channels

The mass balances for the anode and cathode gas channels are

$$\frac{dc^j_{i,k}}{dt} = -\frac{v^j_k c^j_{i,k} - v^j_{k-1} c^j_{i,k-1}}{\Delta z} - \frac{\dot{n}^j_{i,k}}{\delta^j}, \tag{1}$$

where $c^j_{i,k}$ are the concentrations of the different gas species. The transient term on the left side represents accumulation of mass with time and the terms on the

Table 1: Nomenclature

Symbol	Description
Roman letters	
c	Concentration, [mol m^{-3}]
C	Volumetric capacitance, [C V^{-1} m^{-3}]
$CCSA$	Channel cross-section area, [m^2]
$D^{eff}_{i,ks}$	diffusion coefficient, [m^2 s^{-1}]
D_W	Self-diffusion coefficient of water in the membrane, [m^2 s^{-1}]
$ECSA$	Electrode active area, [m^2]
I	Electrical current, [A]
i	Current density, [A m^{-2}]
L	Length, [m]
$\dot{n}$	Molar flux density, [mol m^{-2} s^{-1}]
P	Electrical power, [W]
p	Pressure, [Pa]
r	Reaction rate, [mol m^{-2} s^{-1}]
t	Time, [s]
t_W	Transport number of water in the membrane
T	Temperature, [K]
U	Voltage, [V]
v	Flow velocity, [m s^{-1}]
x	Space coordinate, [m]
y	Space coordinate, [m]
z	Space coordinate, [m]
Greek letters	
δ	Thickness of layer in y-direction, [m]
κ	Electrical conductivity of the membrane, [Ω^{-1} m^{-1}]
Λ	Water content
μ	Electrochemical potential, [J mol^{-1}]
ξ	Mole fraction
ρ	Density, [Kg m^{-3}]
Φ	Electrical potential, [V]
Superscripts	
A	Anode
C	Cathode
j	Indicates A or C
M	Membrane
Subscripts	
i	Gas species
in	Inlet flux
k	Mesh segment

right side of the equation represent the change in mass flow due to convective transport in both z and y directions. The superscript j is used to denote anode side (A) or cathode side (C). The subscript i indicates the species index. On anode side, it can be either H_2 or H_2O. On the cathode side, i can be either O_2, N_2 or H_2O. Gas channel thickness in y-direction is δ^j, $\dot{n}_i^j$ denote molar flow densities between gas channels and gas diffusion layers. Molar flow densities are assumed positive towards the membrane. Subscript $k = 1, 2 \ldots n-1, n$ accounts for segment number. Notice molar mass is used instead of mass. The corresponding boundary equations are

$$v^j c_i^j|_{0,t} = \dot{n}_{i,in}^j, \tag{2}$$

where $\dot{n}_{i,in}^j$ denote inlet molar flow densities (inlet flow divided by cross-sectional area - CCSA of the gas channels).

Following model assumptions, ideal gas law is used to calculate flow pressure in the gas channels, and this equation also relates pressure with total gas concentration

$$p_k^j = RT_k^j \sum_i c_{i,k}^j. \tag{3}$$

The corresponding boundary condition, considering pressure at the outlet of the gas channels is equal to ambient pressure, is

$$p^j\left(L_z, t\right) = p^{amb}. \tag{4}$$

Considering a set of assumptions, such as neglecting the acceleration terms, the Navier-Stokes equation can be simplified into a pressure drop relation [45]. This is how the flow velocity is calculated in the gas channels

$$v_k^j = -K^j \frac{p_{k+1}^j - p_k^j}{\Delta z}. \tag{5}$$

2.2. Molar flux densities from the gas channels to the catalyst layers

Due to model assumptions, hydrogen mass flow from the anode gas channel to catalyst layer is identical to the amount of hydrogen consumed in the anodic reaction $H_2 \rightarrow 2H^+ + 2e^-$:

$$\dot{n}^A_{H_2,k} = r^A_k, \tag{6}$$

where r^A is the rate of the anodic reaction given by the Butler-Volmer equation (detailed in [43]).

The water flow from or to the anode gas channel through the gas diffusion layer depends on membrane water transport

$$\dot{n}^A_{H_2O,k} = \dot{n}^M_{H_2O,k}. \tag{7}$$

The oxygen transported from the cathode gas channel is completely consumed in the cathodic reaction $O_2 + 4e^- + 4H^+ \rightarrow 2H_2O$,

$$\dot{n}^C_{O_2,k} = \frac{1}{2} r^C_k, \tag{8}$$

where r^C is the rate of the cathodic reaction given by the Butler-Volmer equation (detailed in [43]).

Nitrogen flow is zero, since nitrogen is not a reactant and cannot permeate through the membrane,

$$\dot{n}^C_{N_2,k} = 0. \tag{9}$$

Water flow from the cathode is given by the cathode catalyst layer water mass balance,

$$\dot{n}^C_{H_2O,k} = -\dot{n}^M_{H_2O,k} - \frac{1}{2} r^C_k, \tag{10}$$

where $\dot{n}^M_{H_2O,k}$ accounts for drag and back diffusion. Generated water from the electrochemical reaction is represented by the second term on the right side of the equation.

2.3. Water activity in the catalyst layers

The water vapour activity (or water activity) on each side of the membrane is calculated from water partial pressure divided by corresponding saturation pressure according to cell temperature

$$a^{j}_{H_2O,k} = \frac{p^{j}_{k}\xi^{Cj}_{H_2O,k}}{p^{sat}}, \tag{11}$$

where $\xi^{Cj}_{H_2O,k}$ is the mole fraction of water in the catalyst layer obtained from Stefan-Maxwell equations for the gas diffusion layer presented in [43].

Water activity values higher than one indicate condensation on the catalyst layers. In this model, liquid water coverage is approximated by flagging up the presence of condensation when the average of the water activity spatial profile in the anode ($a^{A}_{H_2O,avrg}$) or cathode ($a^{C}_{H_2O,avrg}$) catalyst layer reaches the value one. The water film coverage on each side of the membrane is assumed to decrease reactant access to the electrochemical surface area (ECSA), according to estimated steady-state water coverage ratios in the gas diffusion layers from experimental results reported in [46]. This is a very simple empirical logic developed in this model to account for the effects of accumulated liquid water in the fuel cell, in order to visualise the benefits of control strategies proposed in Section 3. Table 2 shows this empirical function in detail.

In this logic a 5 cm^2-active area single PEM fuel cell example is considered. The ratios of water film coverage at steady-state current values include the effect of water removal by the gas flow rates, therefore ECSA reduction due to water coverage is greater at lower cell current levels. The accumulation time value is 5 seconds, which is representative of rapid duty cycle changes in the operation of the cell, with steady-state behaviour towards the end of the 5-second slot. Active area recovery after a water removal action is not modelled since the focus is on the accumulation rate before such action.

Notice that this logic is a simple, yet feasible, method to approximate the amount of reduction in cell performance (cell current) due to the presence of water in the cell backing layers for a given current level. It is not intended to

Table 2: ECSA approximation function

For both anode and cathode catalyst layers ($j = A, C$):
Set ECSA theoretical value on anode and cathode to 5 cm^2,
Set accumulation timer t_j to zero,
While simulation is running, increment t_j by 1 every second and do:
If $a^j_{H_2O,avrg} \leqslant 1$
    Reset t_j,
else if $a^j_{H_2O,avrg} > 1$ and $t_j > 5$ s
    If $I > 0.5$ A cm^{-2}
        Reduce ECSA by 1% if anode and 0.01% if cathode,
        Reset t_j,
    else if $I > 0.2$ A cm^{-2}
        Reduce ECSA by 2% if anode and 0.05% if cathode,
        Reset t_j,
    else
        Reduce ECSA by 4% if anode and 1% if cathode,
        Reset t_j,
    end
end

accurately model the two-phase flow with this logic, but to establish a common indicator for the performance of different control strategies.

2.4. Polymer electrolyte membrane

Water contents at membrane boundaries to the anode side Λ^{AM} and cathode side Λ^{CM} depend on the water activity in the catalyst layers. Calculation is given by sorption isotherms (80°C)

$$\Lambda^{AM}_k = 0.3 + 12.5\left(a^A_{H_2O,k}\right) - 16\left(a^A_{H_2O,k}\right)^2 + 14.1\left(a^A_{H_2O,k}\right)^3, \qquad (12)$$

$$\Lambda^{CM}_k = 0.3 + 12.5\left(a^C_{H_2O,k}\right) - 16\left(a^C_{H_2O,k}\right)^2 + 14.1\left(a^C_{H_2O,k}\right)^3. \qquad (13)$$

Two different methods of water transport in the membrane are considered, electro-osmotic drag and back diffusion. Electro-osmotic drag is flux of water

molecules transferred from anode to cathode by protons moving through the membrane. The number of water molecules attached to each proton is defined as

$$t_W\left(\Lambda_k\right) = t_W^{Coeff}\frac{\Lambda_k}{22}, \tag{14}$$

where t_W^{Coeff} is the electroosmotic drag coefficient (usually between 2.5 $\pm$ 0.2), and Λ is membrane mean water content (which ranges from 0 to 22 water molecules per sulfonate group). The water drag flux from the anode to the cathode is:

$$\dot{n}_{H_2O,k}^{drag} = t_W\left(\Lambda_k\right)\frac{i_k^M}{F}, \tag{15}$$

where i_k^M is current density of the fuel cell in segment k.

Some water generated on the cathode catalyst layer travels back through the membrane. This is known as "back diffusion", and it usually occurs because the amount of water at the cathode is many times greater than at the anode, resulting in a large concentration gradient across the membrane. The water back diffusion flux can be determined by

$$\dot{n}_{H_2O}^{back} = -\frac{\rho_{dry}}{M_{mem}}D_w\left(\Lambda_k\right)\frac{d\Lambda_k}{dy}, \tag{16}$$

where D_w is the diffusion coefficient expressed as an empirical function of membrane water content for a Nafion 117 membrane [44], ρ_{dry} is the membrane dry density and M_{mem} is its molecular mass. Considering model assumptions, the variation of membrane water content is estimated from equations (12) and (13) as

$$\frac{d\Lambda}{dy} = -\frac{\Lambda_k^A - \Lambda_k^C}{\delta^M}, \tag{17}$$

where δ^M is the thickness of the membrane.

2.4.1. Net water transport through the membrane

The total amount of water flow in the membrane is a combination of the electro-osmotic drag and back diffusion, defined by

$$\dot{n}^{M}_{H_2O} = \dot{n}^{drag}_{H_2O} - \dot{n}^{back}_{H_2O}. \tag{18}$$

2.4.2. Conservation of charge

Current transport is described by governing equations for conservation of charge [47]. Charge balances at the anode and cathode double layers are

$$C^{A}\delta^{CA}\frac{d\Delta\Phi^{A}_{k}}{dt} = i^{M}_{k} - 2Fr^{A}_{k}, \tag{19}$$

$$C^{C}\delta^{CC}\frac{d\Delta\Phi^{C}}{dt} = -i^{M}_{k} + 2Fr^{C}_{k}, \tag{20}$$

where δ^{Cj} represents the thickness of the catalyst layers, r^{A} and r^{C} are the rates of the anode and cathode electrochemical reactions [43].

2.4.3. Potential drop in the membrane

Since the total cell voltage (U) is fixed, the potential drop in the membrane follows from

$$U\left(t\right) = \Delta\Phi^{C}\left(z,t\right) - \Delta\Phi^{M}\left(z,t\right) - \Delta\Phi^{A}\left(z,t\right). \tag{21}$$

In this relation, activation polarisation losses (energy activation barrier) and ohmic losses (potential drop in the membrane) are considered.

2.4.4. Electrical current density

The proton flux through the membrane is driven by gradients of chemical potentials introduced in [43],

$$\dot{n}_{H+,k} = -\frac{\kappa\left(\Lambda_k\right)}{F^2}\bigtriangledown\mu_{H+,k} - \frac{t_W\left(\Lambda_k\right)\kappa\left(\Lambda_k\right)}{F^2}\bigtriangledown\mu_{H_2O,k}, \tag{22}$$

where $\kappa(\Lambda_k)$ is the membrane protonic conductivity as a function of membrane water content Λ [44] in segment k. Electrical current density through the membrane is then related to proton flux by

$$i_k^M = F\dot{n}_{H+,k}, \tag{23}$$

in order to quantify the electrical charge.

2.5. Cell current

In actual fuel cell operation, a small number of electrons (relative to the number of protons) is conducted across the membrane, before combining with the protons at the cathode catalyst layer. However, such loss is neglected in this model given the considered fuel cell current range of operation. Therefore, the total cell current is calculated by integrating the membrane current density along the z-direction,

$$I(t) = L_x \left(\sum_{k=1}^{10} i_k^M \right) L_z, \tag{24}$$

where L_x and L_z are the depth and length of the membrane respectively. Theoretical ECSA is given by $L_x \mathrm{x} L_z$. In this model, a logic was developed to account for liquid water coverage effects, therefore, the actual cell current density is given by

$$I(t) = ECSA_{app} (L_x L_z) \left(\sum_{k=1}^{10} i_k^M \right), \tag{25}$$

where $ECSA_{app}$ is the proportion of active area not covered by accumulated liquid water.

2.6. Model implementation and validation

The set of discretised model equations was implemented and numerically solved with MATLAB Simulink using the ODE15s solver for stiff systems and differential-algebraic equations (DAEs). The model is non-linear with 110 states (ODEs) and 310 algebraic variables. A ten-segment mesh was sufficient to

illustrate smooth spatial profiles and highlight the control challenge. Initial values for each state are determined by a set of initial conditions obtained from the steady-state behaviour of an experimental single PEM fuel cell from Pragma Industries. This cell is available in the fuel cell laboratory of the Robotics and Industrial Informatics Institute, Barcelona, Spain. This is a joint research facility sponsored by the Polytechnic University of Catalonia and the National Spanish Research Council.

The distributed parameter single cell model developed in this chapter has been validated using two approaches. A classic lumped-parameter fuel cell model quantitative validation approach is presented in this section. In this case, physical and empirical parameters of the model were adjusted to meet the specifications of the Pragma fuel cell. In this study, overall cell temperature is controlled to a constant value of 70°C. It is assumed that the temperature of the gas channels will converge to the same temperature level of the MEA components.

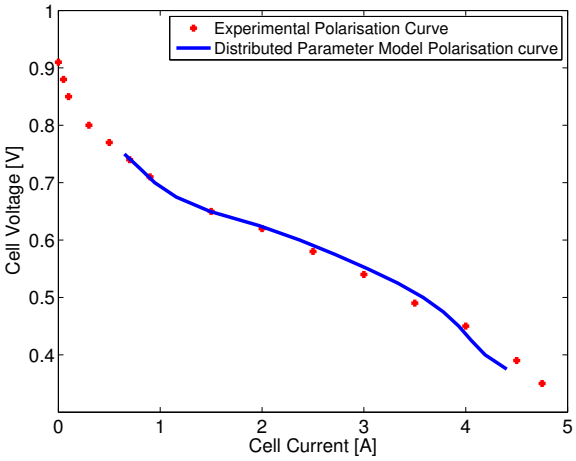

Figure 2: Quantitative validation study - Experimental polarisation curve vs. Model polarisation curve

Notice that the polarisation curve for the model only covers the valid range of operation according to assumptions established. Comparing both polarisation

curves within the range of operation valid for the model, the average absolute current error is 0.053 A. The results indicate that the distributed parameter model gives a good representation of the experimental single PEM fuel cell across a range of steady-state operating points. The accuracy of the model validates mass and energy balances, as well as the cell voltage model.

Validation of spatial profiles within the PEM fuel cell is a very challenging task, due to the lack of sensors to measure such profiles, or if available, the cost and complexity that these sensors add up to the system. Several authors have analysed internal cell behaviour through electrochemical impedance analysis or imaging techniques, which generate important results and conclusions at cell research and development stages [8]. In this work, the second approach used to validate the model consists of a qualitative analysis of the internal spatial profiles of the fuel cell. This approach was presented in Sarmiento-Carnevali et al. [43], a work dedicated to analyse transient and steady-state behaviour of internal variables along the z-direction of the cell.

3. Decentralised distributed parameter model predictive control of water activity

Figure 3 depicts the proposed control scheme. The system to be controlled is the single PEM fuel cell inside the dashed box, represented by the non-linear distributed parameter model described in Section 2. There are 6 inputs to the cell: the voltage U, according to a certain duty cycle, the cooling temperature input that is assumed to be taken care of by a dedicated temperature control loop outside the scope of this control scheme, the hydrogen inlet flux $\dot{n}^{A}_{H_2,in}$ and the anode water inlet flux $\dot{n}^{A}_{H_2O,in}$, which are manipulated variables of the anode MPC, the oxygen/nitrogen inlet flux $\dot{n}^{C}_{air,in}$ and the cathode water inlet flux $\dot{n}^{C}_{H_2O,in}$, which are manipulated variables of the cathode MPC.

The model measured outputs are the cell current I and temperature T. The observed outputs are the water activity profiles on the catalyst layers of the anode $a^{A}_{H_2O,k}$ and the cathode $a^{C}_{H_2O,k}$. These are the controlled variables. The

gas fluxes through the cell are also estimated: $\dot{n}^{A}_{H_2,k}$, $\dot{n}^{A}_{H_2O,k}$, $\dot{n}^{C}_{air,k}$ and $\dot{n}^{C}_{H_2O,k}$, as these profiles are required by the MPC controllers.

The overall control targets of the strategy are (1) to supply the required inlet gas flow according to defined system stoichiometry, (2) to reduce the rate of accumulation of liquid water on the catalyst and other backing layers and (3) to prevent local drying on the membrane or catalyst layers of the anode and cathode, in order to ensure proper membrane protonic conductivity and adequate conditions for the electrochemical reactions to occur. The following sub-sections describe the design and implementation process of this control scheme.

3.1. Design of model predictive controllers

Model predictive control (MPC) is part of the family of the optimisation-based control methods that use on-line optimisation for computation of future control steps. Using a reference model of the plant to be controlled, the optimiser predicts the effect of past inputs on future outputs. The number of predicted output steps is called the prediction horizon. The overall objective of this process is to compute a sequence of future control moves that minimises a certain cost function, which includes penalties on the trajectory of predicted tracking error. The number of steps in the sequence of future control moves is the control horizon. Once estimated, the first step of the sequence is applied and the entire optimisation is repeated from the next step onwards. The size of the steps is known as sampling time of the controller. Output feedback is used to ensure convergence of the controller and to account for potential reference model inaccuracies. The optimisation can be constrained or unconstrained according to the characteristics of the plant to be controlled and the hardware requirements of the manipulated variables. The use of MPC in this work, being a classic model-based approach, allows the consideration of spatial variations of water activity by using distributed parameter models as reference models. Extended details on the MPC control approach can be found in [48].

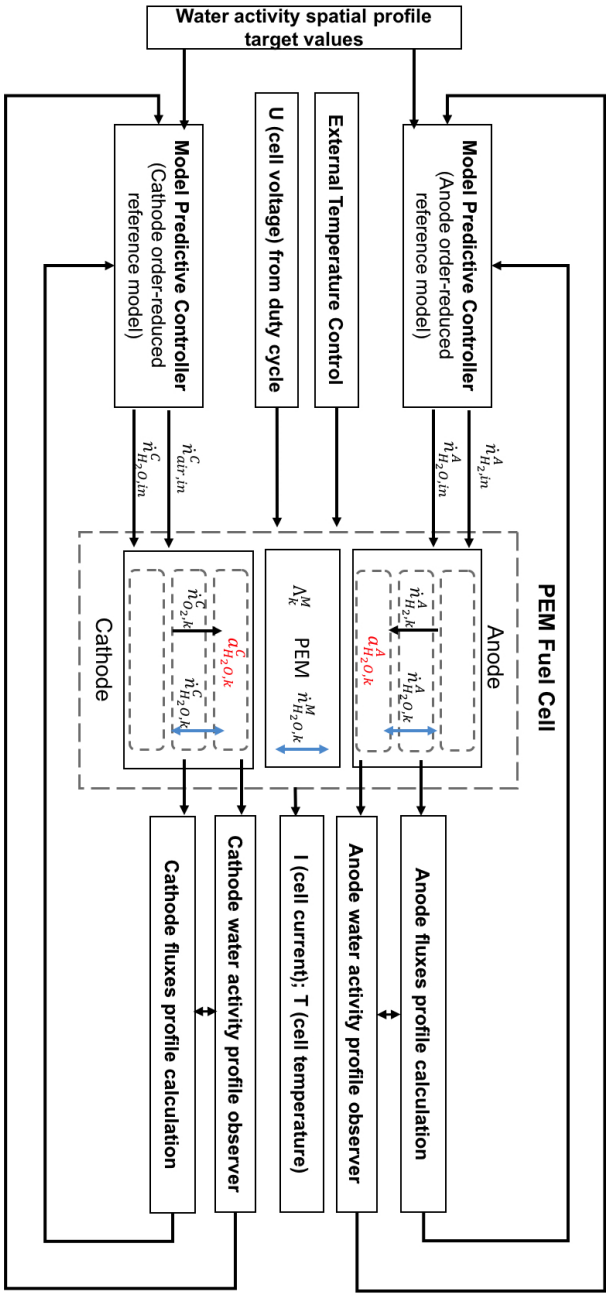

Figure 3: Decentralised distributed parameter model predictive control of water activity

3.1.1. Anode and cathode reference models

The first step in designing the MPC controllers for the current scheme is to define the reference models. Non-linear sub-models for the anode layers and cathode layers are derived from the non-linear model introduced in Section 2. The sub-models are represented by corresponding equations (1-5) and (11). Both models consider ordinary differential equations (ODE) and algebraic equations. Differential algebraic equations (DAE) systems resulting from discretisation of distributed parameter models normally have a large number of equations as appreciated in Section 2. In this study, 10 mesh segments are considered along the z-direction.

It is common practice to neglect spatial variations and consider simplified lumped-parameter models as reference models in control applications, in order to achieve a trade-off between accuracy of the model and computational complexity. However, in this work the spatial profile behaviour is the focus of the control strategy, therefore order-reduced models are used as simplified reference models of the anode and cathode. Corresponding model variables (before order reduction) are:

Anode sub-model.

- States (x_1 vector): $c^A_{H_2,k}$ and $c^A_{H_2O,k}$ ($k = 1..10$),
- Algebraic variables (x_2 vector): p^A_k and v^A_k ($k = 1..10$),
- Inputs (u vector): hydrogen inlet flux $\dot{n}^A_{H_2,in}$ and water inlet flux $\dot{n}^A_{H_2O,in}$,
- Outputs (y vector): water activity in segments $a^A_{H_2O,1}$, $a^A_{H_2O,6}$, $a^A_{H_2O,10}$ and average water activity level $a^A_{H_2O,avrg}$ of the profile along the z-direction.

Cathode sub-model.

- States (x_1 vector): $c^C_{O_2,k}$, $c^C_{N_2,k}$ and $c^C_{H_2O,k}$ ($k = 1..10$),
- Algebraic variables (x_2 vector): p^C_k and v^C_k ($k = 1..10$),

- Inputs (u vector): air inlet flux $\dot{n}^C_{O_2,in}$, $\dot{n}^C_{N_2,in}$ and the cathode water inlet flux $\dot{n}^C_{H_2O,in}$,

- Outputs (y vector): water activity in segments $a^C_{H_2O,1}$, $a^C_{H_2O,6}$, $a^C_{H_2O,10}$ and average water activity level $a^C_{H_2O,avrg}$ of the profile along the z-direction.

The outputs are defined as key values of the water activity profiles of the anode and cathode catalyst layer, i.e. the water activity in the first, middle and last mesh segments. Results shown in Section 5 indicate that these three outputs provide enough information to monitor and control the overall water activity profiles. Each DAE system has the form

$$\begin{aligned} F_1\left(\dot{x}_1, x_1, x_2, u\right) &= 0, \\ F_2\left(x_1, x_2, u\right) &= 0, \\ y - h\left(x_1, x_2, u\right) &= 0, \end{aligned} \tag{26}$$

where $x_1 \in \mathbb{R}^d$ is the state vector, $x_2 \in \mathbb{R}^a$ is the vector of algebraic variables, $u \in \mathbb{R}^r$ is inputs vector, and $y \in \mathbb{R}^q$ is the outputs vector. In addition, the DAE model has an underlying ODE description,

$$\begin{aligned} \dot{x}_1 &= \mathcal{L}\left(x_1, x_2, u\right), \\ x_2 &= \mathcal{R}\left(x_1, u\right), \end{aligned} \tag{27}$$

therefore, it follows that

$$\begin{aligned} \dot{x}_1 &= \mathcal{L}\left(x_1, \mathcal{R}\left(x_1, u\right), u\right), \\ y &= h\left(x_1, \mathcal{R}\left(x_1, u\right), u\right). \end{aligned} \tag{28}$$

After both sub-models are completely defined, balanced truncation is used to reduce their order [49]. This method requires linearising around an equilibrium point of interest, computing the corresponding controllability and observability functions, and finding an appropriate model realisation that reveals which states of the original system can be truncated without considerably affecting the original input-output behaviour. Detailed information of the balanced truncation

technique can be found in [50]. The resulting reference models of the anode and cathode are linear time-invariant models of the form

$$\begin{aligned} \dot{z_a} &= A_{red} z_a + B_{red} u, \\ y &= C_{red} z_a, \end{aligned} \tag{29}$$

where $z_a \in \mathbb{R}^k$ is the state vector, $u \in \mathbb{R}^r$ are the control inputs and $y \in \mathbb{R}^q$ are the outputs. Note that the new set z_a of states has no physical meaning since it is a linear combination of the full order set of states. The inputs and outputs remain the same and, ideally, the internal dynamics of the reduced order model preserves the input-output relation of the original DAE.

Parameter-dependent reference models. A variation of the balanced truncation technique is also used in this work to increase the accuracy of the linear reference models. The result of this technique is an order-reduced model that incorporates the effects of changes in important external variables. Applying this method, the modified reference models consider a parameter m that accounts for temperature deviations from the equilibrium operating point used in the linearisation step. This parameter is considered as a measured disturbance to the MPC controllers,

$$\begin{aligned} \dot{z_a} &= A_{red}\left(m\right) z_a + B_{red}\left(m\right) u, \\ y &= C_{red}\left(m\right) z_a. \end{aligned} \tag{30}$$

Details of this strategy are presented in [51]. The procedure is similar to the sequence of steps followed to obtain the model (29). Figure 4 depicts the results of two options of reference model for anode and cathode. The anode full order nonlinear model has 20 states and the cathode full order nonlinear model has 30 states. For anode and cathode, both kinds of reference models are designed around an equilibrium point of 70°C. At time = 15 s, a step change in temperature from 70°C to 80°C is considered to test the accuracy of the different reference models. Simulations are in open loop. During the first 15 seconds both models show low to zero error in the approximation of the original nonlinear model. After the step change, the parameter-dependent

reference model clearly registers the change in temperature an remains accurate, as temperature deviations from the design setpoint 70°C are taken into account ($m = 10$°C). The reference model obtained through classic balance truncation techniques presents a certain offset, as expected, even though it is designed to have a higher order to cope with temperature variations. However, this reference model has less complexity and this benefit will be analysed in the following sections.

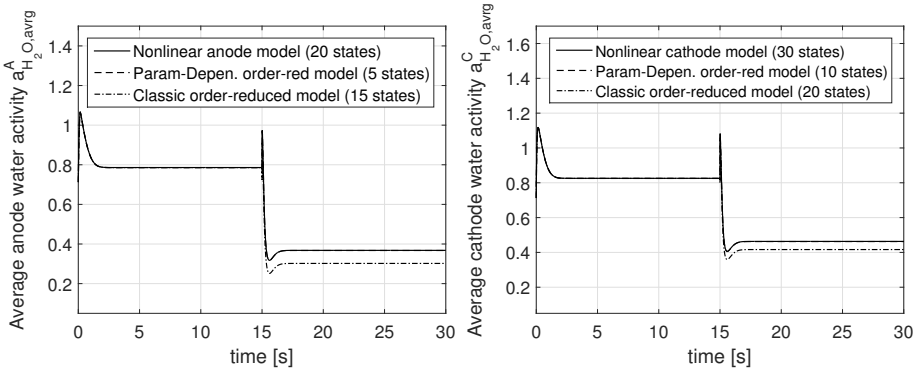

(a) Anode (b) Cathode

Figure 4: Outputs of reference models obtained with different order-reduction techniques vs. corresponding nonlinear fuel cell model outputs. Comparative under a temperature step change.

3.1.2. The MPC optimisation problem

Once the reference model is established, the next step in the design of an MPC controller is to define the cost function and corresponding constraints. The objective function for the MPC controller is the minimisation of the sum of squared errors between the desired setpoint and the actual trajectory of system output, with an additional penalty imposed on rapid changes in the manipulated variables,

$$f(u) = \int_0^{t_h} \left[W \left(y(u,t) - y_{set}(t) \right)^2 \sum_i S_i \left(\frac{\partial u_i}{\partial t} \right)^2 \right] dt. \tag{31}$$

The weight functions, W and S, are used to increase the importance of specific control objectives. The function is discretised over time, obtaining the following algebraic relation

$$f(u) = (y(u) - y_{set})^T W (y(u) - y_{set}) + \sum_i du_i^T S_i du_i. \quad (32)$$

The vector $y(u)$ is the value of the outputs at the different time steps in the prediction horizon, while element i of vector du is the value of u at time step i minus its value at time step $i-1$. The constraints depend on the upper and lower level values of the manipulated variables, as well as the physical limitations imposed by model assumptions. In this subsection the subscript i is used to account for time steps.

3.1.3. MPC design of the cost function

Each MPC has two targets: (i) to provide the correct amount of reactant gases and (2) to maintain proper membrane protonic conductivity and adequate conditions for the electrochemical reactions to occur, whilst reducing the rate of formation and accumulation of liquid water using the knowledge from observed water activity spatial profile results. The overall idea of the MPC controller in this strategy is to efficiently manage the inlet water humidification on both anode and cathode, taking full advantage of the drag and back diffusion fluxes.

Membrane hydration levels are controlled through the water activity setpoints. These setpoints are defined using a previous analysis of the polymer behaviour presented in [46]. This approach is:

- Upon high current levels ($\geqslant 0.5$ A cm^{-2}), anode and cathode catalyst layer water activity setpoints are increased closer to condensation values (0.8. to 1). Using these values the membrane water content is kept within 14 to 22.

- During lower current levels (< 0.5 A cm^{-2}), anode and cathode catalyst layer water activity setpoints are set to vapour water region values (0.6.

to 0.79). Using these values the membrane water content is kept within 8 to 14.

The objective of this setpoint selection approach is to avoid condensation when it is possible to keep the water activity in the vapour region, without affecting the membrane protonic conductivity at different current levels. Table 3 presents the different elements in the cost function of each MPC controller.

Prediction and control horizons for each MPC are 2 and 0.6 seconds respectively. Sampling time is 0.2 seconds. The controller tuning method is described in [48]. Several approaches presented in this reference were tested to guarantee best performance.

3.2. Design of observers

An MPC requires measured output feedback to ensure convergence towards target setpoints. However, some of the chosen outputs are very difficult to measure, such as internal values of the water activity profile on each side of the membrane. In order to address this issue, state observers are designed for both the anode and cathode models to estimate the water activity profile. As the water activity profile is part of the set of algebraic variables, the first step to estimate this profile is to observe the concentration of species on both the anode and cathode channels (1). After estimating these states, the water activity profiles are computed using algebraic equations (3) and (11). In this work only linear observers are designed and implemented. This decision is based on the desire to keep the control system as simple as possible maintaining the main control objectives. Detailed information on observers and the observability concept can be found in [52].

The mathematical model of the observer designed is

$$\tilde{x}_1 = A\tilde{x}_1 + Bu + K_e(y - C\tilde{x}_1) \tag{33}$$

$$= (A - K_eC)\tilde{x}_1 + Bu + K_ey, \tag{34}$$

Table 3: Anode and Cathode MPC design

Anode MPC		
Var.	Description	Comments
$\dot{n}^{A}_{H_2,in}$	Manipulated variable. Range of H_2 stoichiometry values from 1.5 to 2	Corresponding weight is 10, which accounts for high penalisation upon changes from 1.5. Changes are only allowed in low temperature conditions to increase anode pressure.
$\dot{n}^{A}_{H_2O,in}$	Manipulated variable. Range of %RH values from 10 to 85	Corresponding weight is 0, which indicates no penalisation upon changes.
$a^{A}_{H_2O,k}$	Controlled variable	Three segments are considered k = 1, 6 and 10. Restricted from 0.2 to 1 with 0.3 weight value indicating flexible setpoint
$a^{A}_{H_2O,avrg}$	Controlled variable	Restricted from 0.65 to 1 with weight value 1 indicating high priority to meet setpoint defined by current level
$\dot{n}^{A}_{H_2,k}$	Estimated disturbance	The complete 10-element profile is consider a known disturbance as it is computed from the anode observer results
$\dot{n}^{A}_{H_2O,k}$	Estimated disturbance	The complete 10-element profile is consider a known disturbance as it is computed from the anode observer results
Cathode MPC		
$\dot{n}^{C}_{air,in}$	Manipulated variable. Range of O_2 stoichiometry values from 2 to 3	Corresponding weight is 10, which accounts for high penalisation upon changes from 2. Changes are only allowed in low temperature conditions to increase cathode pressure.
$\dot{n}^{C}_{H_2O,in}$	Manipulated variable. Range of %RH values from 10 to 85	Corresponding weight is 0, which indicates no penalisation upon changes.
$a^{C}_{H_2O,k}$	Controlled variable	Three segments are considered k = 1, 6 and 10. Restricted from 0.2 to 1 with 0.3 weight value indicating flexible setpoint
$a^{C}_{H_2O,avrg}$	Controlled variable	Restricted from 0.65 to 1 with weight value 1 indicating high priority to meet setpoint defined by current level
$\dot{n}^{C}_{O_2,k}$	Estimated disturbance	The complete 10-element profile is consider a known disturbance as it is computed from the anode observer results
$\dot{n}^{C}_{H_2O,k}$	Estimated disturbance	The complete 10-element profile is consider a known disturbance as it is computed from the anode observer results

where $\tilde{x}_1$ is the estimated state and $C\tilde{x}$ is the estimated output. The inputs of the observer are the system output y and the system control inputs u (manipulated variables). The matrix K_e, known as the *observer gain matrix*, is a weight matrix for the correction term that involves the difference between the measured output and the observed output $C\tilde{x}$. This term continually corrects the observer output improving its behaviour.

Figure 5 shows the performance of both anode and cathode observers. For simplicity, only the average water activity is presented. Step changes in voltage, from 0.65 V to 0.55 V at 0.1 s and from 0.55 V to 0.75 V at 0.3 s, are used to test observer robustness. Notice that the observer error converges to zero shortly before 0.1 seconds, which is half the sampling time of the MPC controllers. This condition is desirable to ensure the observer is faster than the controller and accurate predictions are fed into the optimiser.

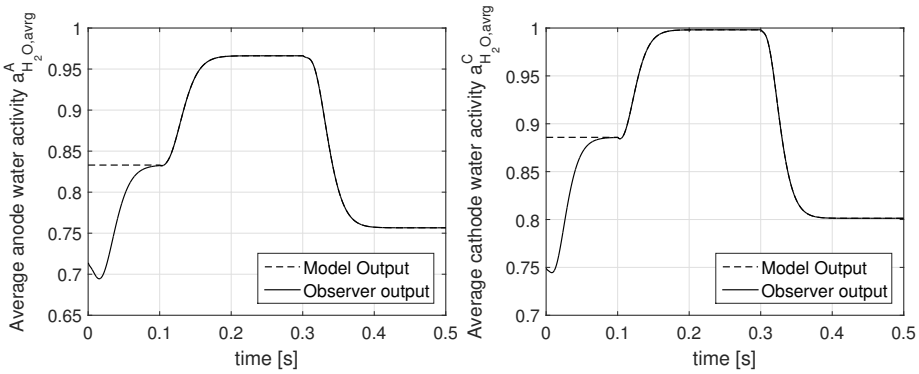

(a) Anode (b) Cathode

Figure 5: Anode (a) and cathode (b) observer outputs vs. corresponding nonlinear fuel cell model outputs under voltage step changes

It is also necessary to estimate the variables $\dot{n}^A_{H_2,k}$, $\dot{n}^A_{H_2O,k}$, $\dot{n}^C_{O_2,k}$, $\dot{n}^C_{N_2,k}$ and $\dot{n}^C_{H_2O,k}$ $(k = 1..10)$. The same approach is used for this estimation. Once the state observation is accomplished, algebraic equations (6-10) are used to calculate corresponding variables.

3.3. MPC design variation considering concentration of reactants as targets

The main objective of this control approach is to avoid starvation of reactants in both anode and cathode catalyst layers. This is achieved by controlling the concentration of reactants in the outlet end of the gas channels. The control target is to prevent zero or negative concentration values. Higher levels of reaction rate occur towards the gas inlet end of the channels where reactants partial pressure is higher. Therefore, the last segments along the z-direction are more vulnerable to starvation. However, starvation could occur anywhere along the flow direction due to the presence of liquid water or degradation issues, which makes a spatial control approach the proper to prevent such problems.

In this study, only concentrations in the last mesh segment (number 10) of the anode and cathode gas channels are controlled. This target is achieved by including a constraint in the MPC optimisation process to prevent concentration variables from reaching zero values. Table 4 shows the variations included in the previous design of both controllers in order to implement this strategy. The same approach could be implemented for the control of the concentrations in any other segment or various segments along the gas channels.

4. Definition of control strategies

Three different decentralised distributed parameter model predictive control (DPMPC) strategies were implemented considering the steps presented in Section 3. Summary and most relevant features are:

- **DPMPC-1**: this strategy is focused on the control of observed water activity profiles along the z-direction of the anode and cathode catalyst layers, as well as hydrogen and oxygen stoichiometry levels. The MPC controllers have parameter-dependent reference models presented in Section 3.1.1. Spatial control of observed reactant concentrations is not included.

- **DPMPC-2**: this strategy is focused on the spatial control of water activity profiles along the z-direction of the anode and cathode catalyst layers,

Table 4: Anode and Cathode MPC design variation to implement control of gas concentrations

Anode MPC design changes		
Var.	Description	Comments
$\dot{n}^{A}_{H_2,in}$	Manipulated variable. Range of stoichiometry values from 1.5 to 2	Corresponding weight is 10, which accounts for high penalisation upon changes from 1.5. Changes are only allowed in low temperature conditions to increase anode pressure or to meet hydrogen concentration setpoint target towards channel outlet.
$c^{A}_{H_2,10}$	Controlled variable	Channel outlet hydrogen concentration restricted to have positive values only
Cathode MPC design changes		
$\dot{n}^{C}_{air,in}$	Manipulated variable. Range of stoichiometry values from 2 to 3	Corresponding weight is 10, which accounts for high penalisation upon changes from 2. Changes are only allowed in low temperature conditions to increase cathode pressure or to meet oxygen concentration setpoint target towards channel outlet.
$c^{C}_{O_2,10}$	Controlled variable	Channel outlet oxygen concentration restricted to have positive values only

as well as spatial control of observed reactant concentrations in the last mesh segment. The MPC controllers have parameter-dependent reference models presented in Section 3.1.1.

- **DPMPC-3**: this strategy is focused on the spatial control of observed water activity profiles along the z-direction of the anode and cathode catalyst layers, as well as hydrogen and oxygen stoichiometry levels. The difference in comparison to DPMPC-1 is the use of classic balance truncation to design the reference models of the MPC controllers. Spatial control of observed reactant concentrations is not included.

5. Simulation results and discussion

The non-linear PEM fuel cell model and the three different control strategies presented in Section 4 are analysed via simulation environment in MATLAB Simulink. Three tests have been designed. The first test focuses on the control of water activity profiles along the z-direction of the anode and cathode

catalyst layers. The objective of this test is to compare DPMPC-1 to a classic inlet gas humidification strategy. The second test focuses on the control of the concentration of reactants along the z-direction of the gas channels. The objective of this test is to compare DPMPC-1 vs. DPMPC-2. Finally, the third test aims at comparing the effect of parameter-dependent reference models in the performance of the overall control strategy. The objective of this test is then to compare DPMPC-1 vs. DPMPC-3.

5.1. Analysis of DPMPC-1 vs. classic inlet gas humidification control

This test compares the performance of DPMPC-1 to a traditional current-based humidification approach that fixes the anode inlet gas relative humidity to 50%, and the cathode inlet gas relative humidity to 30% for the different steps in a duty cycle. In this approach humidification increases or decreases with current according to the fixed stoichiometry. Such approach is the baseline humidification control strategy.

Transient-state results. A voltage cycle is designed including three different operating regions to test and analyse the performance of DPMPC-1. Figure 6 shows different results of this test. Figure 6a presents the voltage cycle under analysis. Voltage levels considered range from 0.55 V to 0.75 V, which correspond to 43.9% up to 59.9% low hydrogen heating value (LHV) fuel cell efficiency. A square wave is chosen to assess the control performance upon step changes. Voltage value is updated every 5 seconds. This time frame is similar to average time for changes in duty cycles of applications like automotive (WLTP driving cycle, for example) [53], and allows the evaluation of control convergence. First operating point corresponds to $U = 0.65$ V, which is the average cell operating point (equilibrium point for MPC controllers design). Operating points $U = 0.55$ V and $U = 0.75$ V represent high and low currents respectively. Cell temperature is assumed to be kept around 70°C during the simulation. Table 5 shows the simulation parameters considered for this study.

Total cell current is shown in Figure 6b. Figures 6c and 6d indicate the average water activity level on anode and cathode sides of the membrane ($a^{A}_{H_2O,avrg}$

Table 5: Simulation parameters

Symbol	Description
C^A	8.25 x 10^6 F m^{-3}
C^C	8.25 x 10^6 F m^{-3}
$CCSA$	8.75.10^{-7} m^2
$D^{eff}_{H_2,H_2O}$	10^{-6} m^2 s
$D^{eff}_{O_2,H_2O}$	3 x 10^{-6} m^2 s
$D^{eff}_{O_2,N_2}$	2 x 10^{-6} m^2 s
$D^{eff}_{H_2O,N_2}$	2.5 x 10^{-6} m^2 s
δ^A	0.7x10^{-3} m
δ^{AC}	4x10^{-5} m
δ^C	0.7x10^{-3} m
δ^{GA}	0.34x10^{-3} m
δ^{GC}	0.34x10^{-3} m
δ^{CC}	1.1x10^{-4} m
δ^M	1.75x10^{-4} m
$ECSA$	0.0005 m^2
K^A	10^{-5} m^2 s^{-1} Pa^{-1}
K^C	10^{-4} m^2 s^{-1} Pa^{-1}
L_x	0.00125 m
L_z	0.4 m
p^{amb}	101325 Pa

and $a^C_{H_2O,avrg}$), which are the controlled variables with highest weight in the optimisation process of each MPC controller. The impact of the proposed control strategy is appreciated in these two figures. Notice how condensation is delayed by DPMPC-1 in comparison to the baseline strategy at time = 10 s, by focusing on the observed water activity profile instead of maintaining a constant humidification level. The importance of observing the behaviour of the spatial profile of water is highlighted in this result.

Figures 6e and 6f show the behaviour of inlet fluxes of water in both anode and cathode explaining the difference in the humidification approach. During the first 10 seconds of the simulation, voltage steps 0.65 V and 0.7 V, both strategies behave similarly regarding cell performance. However, the baseline control strategy always inputs a certain amount of water to maintain a humidification level proportional to the current. Therefore, at this voltage levels the average water activity can even be less than DPMPC-1 setpoint. This action

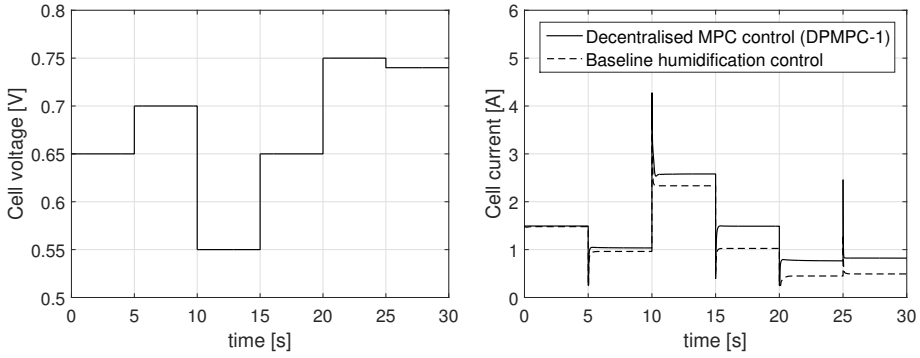

(a) Voltage cycle (b) Total current

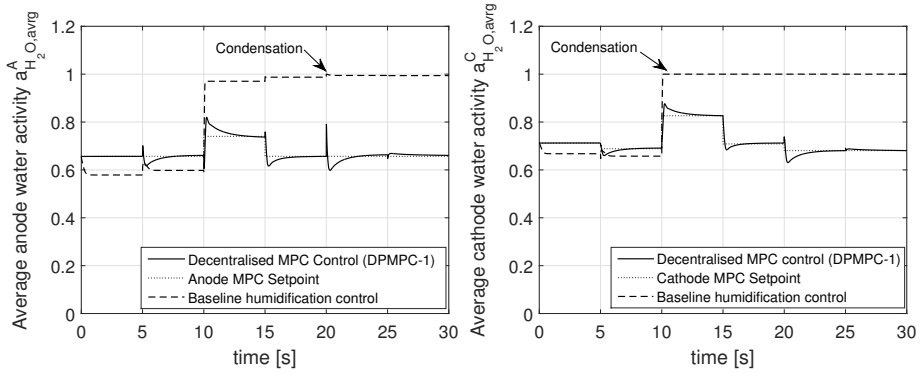

(c) Anode $a^A_{H_2O,avrg}$ (controlled var.) (d) Cathode $a^C_{H_2O,avrg}$ (controlled var.)

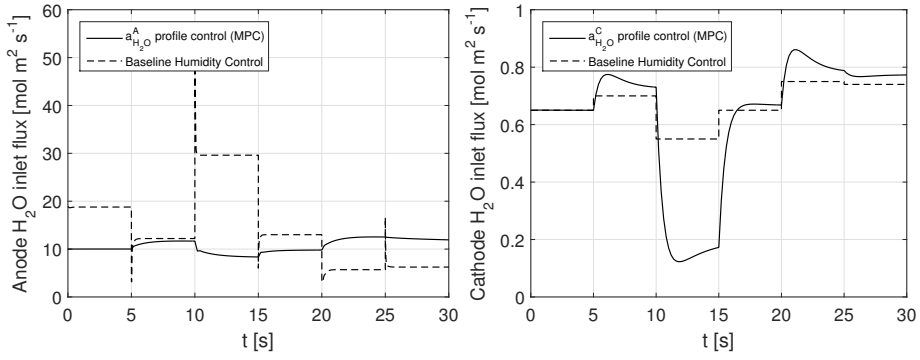

(e) Anode $a^A_{H_2O,in}$ (manipulated var.) (f) Cathode $a^C_{H_2O,in}$ (manipulated var.)

Figure 6: Dynamic results - Voltage Cycle - DPMPC-1 vs. Baseline humidification control strategy

seems intuitively correct in the presence of normal to low current levels (around 0.3 A cm^{-2}), but it is also very likely that in these conditions local drying in the anode occurs if back diffusion levels along the z-direction are not sufficient to compensate water leaving the anode due to the electro-osmotic drag effect.

Upon the step voltage 0.55 V at time = 10 s, the cell operates at high current levels (around 0.7 A cm^{-2}). Clearly, the rate of water generation on the cathode side is very high. In this scenario, DPMPC-1 is able to reduce the accumulation of liquid water by controlling the average water activity to take advantage of generated water, and the back diffusion effect, to properly humidify both the cathode and the anode. During these 5 seconds at high current level, the average water activity setpoints are adjusted to account for major increase in water generation and allow higher membrane humidification levels (as explained is Section 3.1.3). This high current level scenario represents the most challenging task in water management. Excess of accumulated liquid water in the fuel cell layers reduces access of reactants to the active platinum reaction sites (ECSA), and consequently decreases the cell performance, in the worst case causing cell flooding, a major reason of cell failure. Several control systems consider different approaches for liquid water removal, however, the majority of these actions cause either a disruption in the power supplied by the cell, increased parasitic losses or reduction of cell efficiency [5]. The strategy DPMPC-1 reduces the rate of accumulated water in the catalyst layer decreasing the frequency of removal actions and mitigating cell flooding.

Figures 6e and 6f also show the behaviour of the manipulated variables during high current levels (time = 10 to 15 s). Both manipulated variables have around 5 seconds of settling time. The design parameters of each MPC defined in Section 3 prove to be adequate in order to ensure stability. The difference in each approach is clear from these figures. The baseline strategy changes the rate of inlet water flux on the anode and cathode gas channel inlet according to the current level, which is again intuitively a correct action as the electro-osmotic forces may cause dryness in the anode if not properly humidified. On the cathode side, this strategy registers the effect of generated water depending

on current level. However, the baseline strategy aims to maintain a certain humidification level of the inlet gases that results in higher amount of inlet water than necessary leading to condensation on both sides of the membrane. Under low ambient temperature conditions, a traditional current-based humidification approach could increase the chances of local or total flooding, particularly on the anode side.

Notice how DPMPC-1 control action is able to maintain the average water activity level under 1 (Figures 6c and 6d), indicating less liquid water formation and reducing the number of reaction sites affected by liquid water blockage. Following the high current level scenario (beyond 15 s), the impact of DPMCP-1 on the performance of the fuel cell is clearly appreciated (Figure 6b). Decreased current levels due to the presence of liquid water are shown. At this point, most control strategies would trigger a liquid water removal action, like a blowdown or a purge to regain cell performance. Some of these strategies are triggered more or less frequently depending on the amount of current drawn from the cell [54].

Steady-state results. The behaviour of controlled variables with less weight in the optimisation process ($a^A_{H_2O,1}$, $a^A_{H_2O,6}$, $a^A_{H_2O,10}$, and $a^C_{H_2O,1}$, $a^C_{H_2O,6}$, $a^C_{H_2O,10}$) is appreciated in Figure 7. Figures 7a and 7b show-steady state values of the entire water activity spatial profile for both anode and cathode upon high current scenarios (time = 14 s). Liquid water formation is prevented in the anode and considerably decreased in the cathode with DPMPC-1. Condensation is observed at the gas outlet end of the z-direction where it is more challenging to control, as the partial pressure of water tends to be higher due to less reactants concentrations.

In the presence of high current densities, sometimes it is also possible to see anode local drying due to increased electro-osmotic drag [5, 55]. The possibilities of this scenario are reduced by DPMPC-1 as it aims to maintain a healthy water activity level at the inlet throughout the duty cycle. This preventive behaviour decreases the possibility of membrane drying and its degradation consequences.

Figures 7c and 7d correspond to water activity steady state results at low current levels along the z-direction (time = 9 s) for anode and cathode respectively. Notice how the anode water activity shows a tendency towards dryness in the first part of the catalyst layer. This condition occurs because current density is typically higher at channel inlet [56, 57], due to higher reactant partial pressure that results in larger electro-osmotic drag from the anode. Conversely, towards the end of the channel hydrogen partial pressure decreases and there is increased back diffusion of the water that has built up on the cathode. This impact is reduced by DPMPC-1 as it aims to maintain a healthier water activity level at the inlet, reducing the possibility of membrane drying and its degradation consequences.

Finally, Figures 7e and 7f show the membrane hydration levels for both high and low current densities scenarios (t = 14 s and t = 9 s respectively). It can be seen how the baseline humidification control approach keeps the membrane fully hydrated at high current density scenarios due the increased rate of liquid water production. However, during periods of low current densities, unless the fuel cell has been running at higher current densities to generate a certain amount of water, membrane behaviour towards dryness is observed.

Overall, the approach DPMPC-1 has low computational complexity, i.e. 30% CPU capacity in a 2.7 GHz Intel Core i5 processor, which allows for very fast simulation times. It is expected that this approach implemented in a device with high computational capabilities, such as a vehicle electronic control unit (ECU), will have very high performance.

5.2. Analysis of DPMPC-1 vs. DPMPC-2

In the previous section, water activity spatial profiles on both anode and cathode sides of the membrane were controlled to reduce the accumulation of liquid water on the catalyst layers (DPMPC-1). The hydrogen and oxygen stoichiometries were fixed to 1.5 and 3 respectively. This strategy was achieved by restricting the inlet H_2 and O_2 manipulated variables in each MPC to supply only this amount of reactants in proportion to current demanded. In this section,

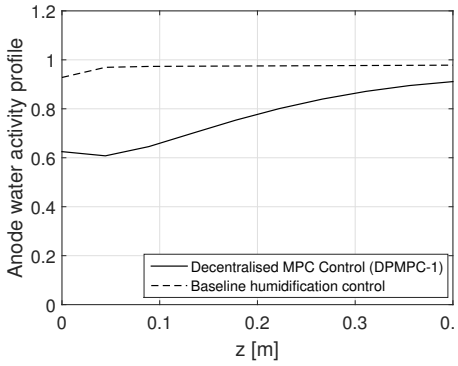

(a) High current density scenario t = 14 s

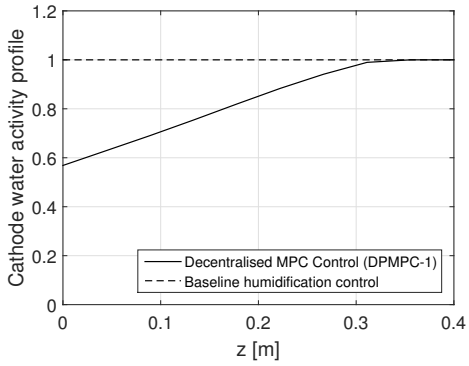

(b) High current density scenario t = 14 s

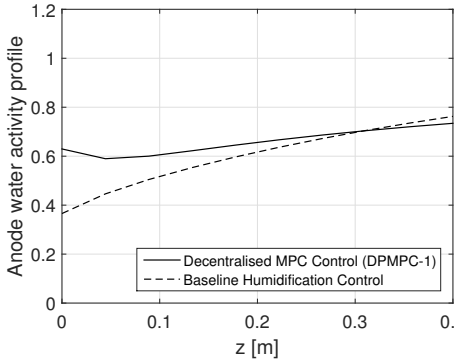

(c) Low current density scenario t = 9 s

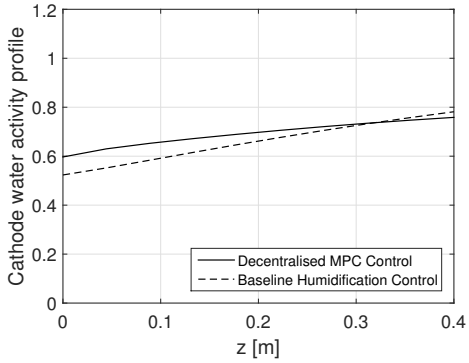

(d) Low current density scenario t = 9 s

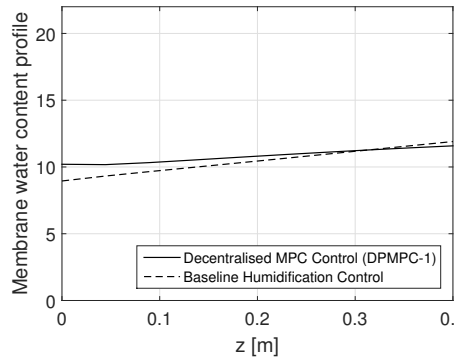

(e) Low current density scenario t = 9 s

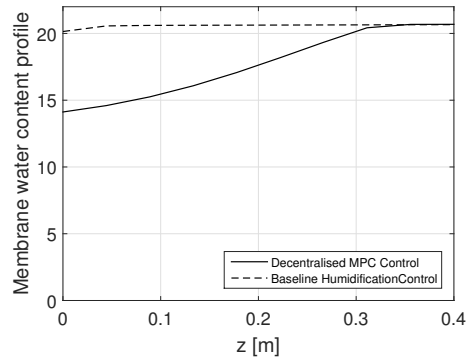

(f) High current density scenario t = 14 s

Figure 7: Steady-state results - DPMPC-1 vs. Baseline humidification control

new spatial control targets are considered in order to exploit the benefits of decentralised distributed parameter control (DPMPC-2). The details of the design for this strategy are presented in Section 3.3.

Figure 8 shows steady-state results of the hydrogen and oxygen concentration profiles along the z-direction for DPMPC-1 vs. DPMPC-2 under the operating point $U = 0.55$ V. The results not only confirm the preventive effect of the control actions on the gas concentrations in the last segment of the channel, but also demonstrate the overall impact of the strategy along the concentration spatial profiles.

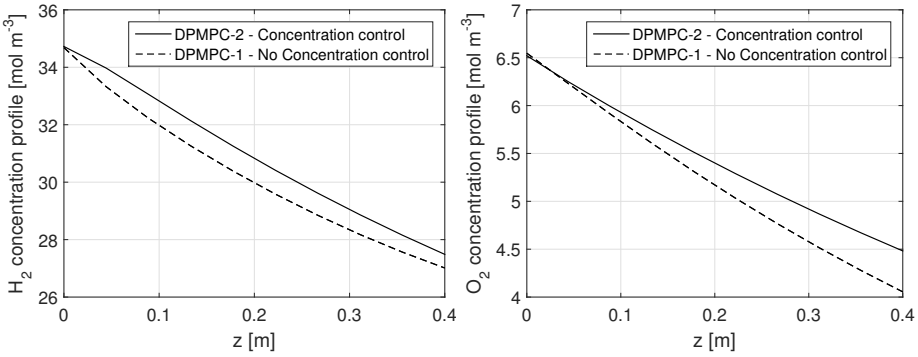

(a) (b)

Figure 8: Steady-state results - High current scenario - Control of reactants concentration in the last segment along the z-direction

5.3. Analysis of DPMPC-1 vs. DPMPC-3

Changes in voltage and temperature are the most important external disturbances to the controlled PEM fuel cell under study. A test is designed to specifically assess the robustness of the proposed control strategies DPMPC-1 vs. DPMCP-3 under different temperature conditions. Figure 9 shows the results of the two versions of DPMPC under a temperature cycle (Figure 9a). Temperature is a key variable to demonstrate control robustness, as the linear reference models depend on a fix equilibrium point (70°C) when created (Section 3). However, DPMPC-1 considers the deviation of temperature from the

original equilibrium point as a measured disturbance. DPMPC-3 does not hold this characteristic in order to make it a much faster controller. This advantage allows the reference models in DPMPC-1 to remain accurate under different temperature conditions. This figure clearly shows the better performance of DPMPC-1 for temperature fluctuations.

Temperature has a clear impact on pressure, affecting both current (Figure 9b) and the water activity profile. Model inaccuracies of DPMPC-3 are observed during this temperature cycle. The changes in pressure appreciated through temperature changes are not understood by the corresponding reference models in DPMPC-3. The control strategy is not able to achieve the average water activity target for both MPC controllers, although it manages to take actions to delay liquid water formation as much as possible (Figures 9c and 9d). DPMPC-1 on the other hand is able to achieve the target in water activity during the simulation time except for 5 seconds where the temperature increases up to 80°C and there is a certain offset in the anode average water activity setpoint. In this case back diffusion is not enough to maintain the desired target and there should be higher control effort from the manipulated variables according to the temperature level. This is one of the most challenging scenarios for water management.

Notice that under extreme external operating conditions (ambient temperature, ambient relative humidity) or extreme duty cycles, inlet gas humidification control strategies, as well as thermal management strategies, might struggle to meet desired control setpoints. This situation will require the action of a master fuel cell system control in order to bring the different variables of the fuel cell back to acceptable operating conditions.

Steady-state results during increased temperature operating conditions (t = 9 s) and decreased temperature conditions (t = 19 s) are analysed in Figures 9e and 9f. The advantage of DPMPC-1 over DPMPC-3 is clear. Figure 9e indicates that DPMPC-3 is not able to cope with a positive deviation of temperature levels from the equilibrium point used in corresponding reference models design. Tendency to dryness in the membrane is noticed. The opposite situation occurs

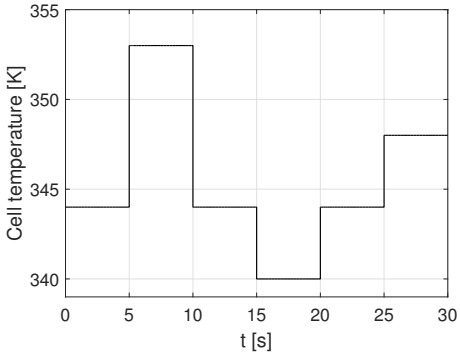

(a) Temperature cycle

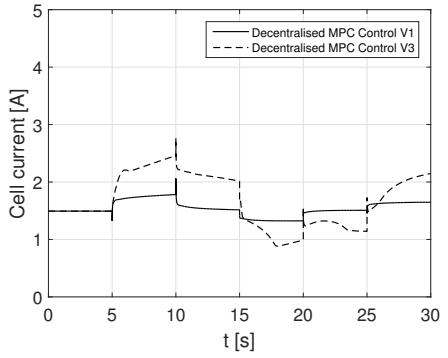

(b) Total current

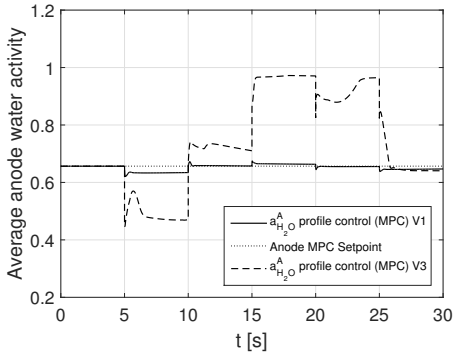

(c) Anode $a^A_{H_2O,avrg}$ (controlled var.)

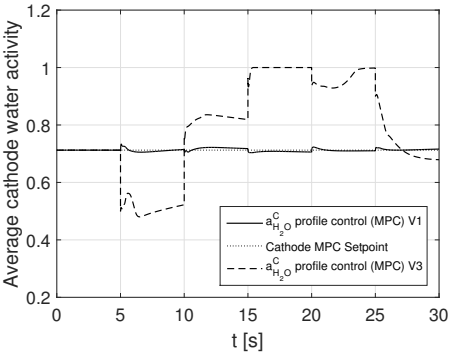

(d) Cathode $a^C_{H_2O,avrg}$ (controlled var.)

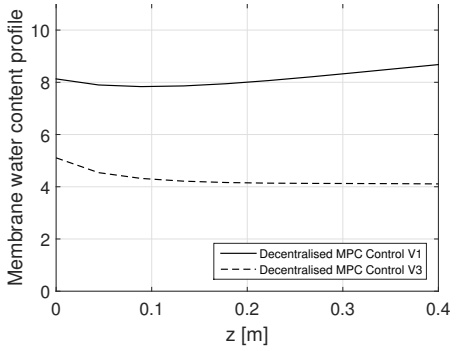

(e) Membrane water content (high temp.)

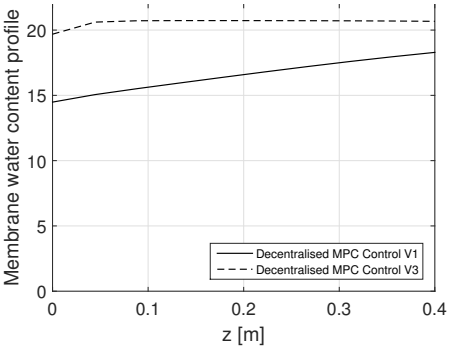

(f) Membrane water content (low temp.)

Figure 9: Temperature Cycle - DPMPC-1 vs. DPMPC-3

upon temperature decrease. Negative deviations from the equilibrium point result in excess liquid water formation keeping the membrane under high water

content levels along the z-direction.

6. Conclusions and on-going extended work

A novel decentralised distributed parameter model predictive control strategy has been designed, implemented and analysed in this work via simulation environment. The control targets focus on supplying the required humidified inlet gas flow whilst reducing the rate of accumulation of liquid water on the catalyst and other backing layers, as well as preventing local drying on the membrane or catalyst layers of the anode and cathode. Spatial control of the concentration of gases is also considered to avoid reactant starvation. The main features of this strategy are:

(1) The use of two separate model predictive controllers (MPC) based on order-reduced models of the anode and cathode to maintain the water activity on both sides of the membrane at appropriate levels, in order to avoid local excess of liquid water or drying. This decentralised condition allows for simpler and faster controllers given the decreased complexity of the reference model in each controller.

(2) The use of distributed parameter models as reference models within the MPC controllers. This allows consideration of water activity and reactants concentration spatial profiles along the z-direction, which are the control targets of this work.

(3) The use of parameter-dependent order-reduced reference models. This allows for more accurate reference models that can adapt to disturbances, increasing the overall control strategy robustness whilst maintaining the simplicity of linear reference models.

(4) The use of observers to estimate the spatial profiles of the different variables of interest and feed these profiles to the MPC controllers. This task is very important for future experimental work since the inclusion of sensors to obtain spatial profiles measures would increase the complexity and

cost of both the system and the controller. Currently, observer design techniques are quite attractive in the analysis of sensorless applications with cost reduction purposes.

Results show an important improvement in cell performance due to reduced liquid water formation rates. The MPC controllers manage to take advantage of the water transport processes within the PEM fuel cell, namely, water generation on the cathode side, electro-osmotic drag due to proton flux through the membrane and back diffusion caused by gradients in water concentration. This feature allows for efficient use of external humidification variables. In addition, proper setpoints chosen to control water activity levels on both anode and cathode catalyst layers result in appropriate membrane humidification levels. Overall, the strategy decreases the loss of performance due to liquid water coverage, as well as the chances for starvation of reactants. The key objective of this approach is to decrease the frequency of water removal actions that cause disruption in the power supplied by the cell, increased parasitic losses and reduction of cell efficiency.

Currently, other possibilities of water activity diagnosis in the fuel cell and different control techniques for the decentralised scheme, as well as a centralised variation, are active tasks in this framework. Future work also includes experimental testing of this concept in order to evolve the approach to higher technology readiness levels.

Acknowledgements

This work was partially funded by Spanish MEC-FPU [grant number AP-2010-3969]; and the Spanish national project MICAPEM (DPI2015-69286-C3-2-R, MINECO/FEDER).

References

[1] Iberdrola, Innovation Report, 2010.

[2] Intelligent Energy Holdings plc, Intelligent Energy has signed a stationary power deal with US-based Luxfer-GTM Technologies as part of a growing strategic relationship in the development of a line of integrated fuel cell products., Accessed on February 20^{th}, 2017.
URL http://www.intelligent-energy.com/news-and-events/company-news/

[3] U.S. Department of Energy, Hydrogen Data Book (2017).
URL http://hydrogen.pnl.gov/hydrogen-data/hydrogen-consumption

[4] H. Li et al., A review of water flooding issues in the proton exchange membrane fuel cell, Journal of Power Sources 178 (1) (2008) 103 – 117. doi:http://dx.doi.org/10.1016/j.jpowsour.2007.12.068.

[5] W. Schmittinger, A. Vahidi, A review of the main parameters influencing long-term performance and durability of PEM fuel cells, Journal of Power Sources 180 (1) (2008) 1 – 14. doi:http://dx.doi.org/10.1016/j.jpowsour.2008.01.070.

[6] J. Le Canut, R. M. Abouatallah, D. A. Harrington, Detection of membrane drying, fuel cell flooding, and anode catalyst poisoning on PEMFC stacks by electrochemical impedance spectroscopy 153 (5) (2006) A857–A864. doi:10.1149/1.2179200.

[7] Y. Sone, P. Ekdunge, D. Simonsson, Proton conductivity of Nafion 117 as measured by a four-electrode AC impedance method, Journal of The Electrochemical Society 143 (4) (1996) 1254–1259. arXiv:http://jes.ecsdl.org/content/143/4/1254.full.pdf+html, doi:10.1149/1.1836625.

[8] S. Cruz-Manzo, R. Chen, P. Rama, Study of current distribution and oxygen diffusion in the fuel cell cathode catalyst layer through electrochemical impedance spectroscopy, International Journal of Hydrogen Energy 38 (3) (2013) 1702 – 1713.

[9] A. Miege, F. Steffen, T. Luschtinetz, S. Jakubith, M. Freitag, Real time water detection for adaptive control strategy in PEMFC-systems, Energy Procedia 29 (2012) 431 – 437, wHEC 2012 Conference Proceedings ? 19th World Hydrogen Energy Conference. doi:http://dx.doi.org/10.1016/j.egypro.2012.09.050.

[10] R. Satija, D.L. Jacobson, M. Arif, S.A. Werner, In situ neutron imaging technique for evaluation of water management systems in operating PEM fuel cells, Journal of Power Sources 129 (2) (2004) 238 – 245. doi:http://dx.doi.org/10.1016/j.jpowsour.2003.11.068.

[11] D. Spernjak, A. Prasad, S. Advani, Experimental investigation of liquid water formation and transport in a transparent single-serpentine PEM fuel cell, Journal of Power Sources 170 (2) (2007) 334 – 344. doi:http://dx.doi.org/10.1016/j.jpowsour.2007.04.020.

[12] R. K. Phillips, B. R. Friess, A. D. Hicks, J. Bellerive, M. Hoorfar, Ex-situ measurement of properties of gas diffusion layers of PEM fuel cells, Energy Procedia 29 (2012) 486 – 495, wHEC 2012 Conference Proceedings ? 19th World Hydrogen Energy Conference. doi:http://dx.doi.org/10.1016/j.egypro.2012.09.057.

[13] T. Van Nguyen, M.W. Knobbe, A liquid water management strategy for PEM fuel cell stacks, Journal of Power Sources 114 (1) (2003) 70 – 79. doi:http://dx.doi.org/10.1016/S0378-7753(02)00591-8.

[14] J. P. Owejan, J. J. Gagliardo, J. M. Sergi, S. G. Kandlikar, T. A. Trabold, Water management studies in PEM fuel cells, part i: Fuel cell design and in situ water distributions, International Journal of Hydrogen Energy 34 (8) (2009) 3436 – 3444. doi:http://dx.doi.org/10.1016/j.ijhydene.2008.12.100.

[15] C.R. Buie et al., Water management in proton exchange membrane fuel cells using integrated electroosmotic pumping, Journal of Power Sources

161 (1) (2006) 191 – 202. doi:http://dx.doi.org/10.1016/j.jpowsour.2006.03.021.

[16] A. Vega-Leal, F. Rogelio-Palomo, F. Barragn, C. Garca, J. Brey, Design of control systems for portable PEM fuel cells, Journal of Power Sources 169 (1) (2007) 194 – 197. doi:http://dx.doi.org/10.1016/j.jpowsour.2007.01.055.

[17] J. Ahn, S. Choe, Coolant controls of a PEM fuel cell system, Journal of Power Sources 179 (1) (2008) 252 – 264. doi:http://dx.doi.org/10.1016/j.jpowsour.2007.12.066.

[18] B. Balasubramanian, F. Barbir, J. Neutzler, Optimal operating temperature and pressure of PEM fuel cell systems in automotive applications, Energy Partners, L.C. New Orleans (Paper 0977).

[19] D. Feroldi, M. Serra, J. Riera, Performance improvement of a PEMFC system controlling the cathode outlet air flow, Journal of Power Sources 169 (1) (2007) 205 – 212. doi:http://dx.doi.org/10.1016/j.jpowsour.2007.01.053.

[20] F. Zenith, S. Skogestad, Control of fuel cell power output, Journal of Process Control 17 (4) (2007) 333 – 347. doi:http://dx.doi.org/10.1016/j.jprocont.2006.10.004.

[21] J. Pukrushpan, A. Stefanopoulou, H. Peng, Modeling and control for PEM fuel cell stack system, in: Proceedings of the American Control Conference, Vol. 4, 2002, pp. 3117–3122.

[22] C. Woo, J. Benziger, PEM fuel cell current regulation by fuel feed control, Chemical Engineering Science 62 (4) (2007) 957 – 968. doi:http://dx.doi.org/10.1016/j.ces.2006.10.027.

[23] C. Wang, H. Nehrir, H. Gao, Control of PEM fuel cell distributed generation systems, in: 2006 IEEE Power Engineering Society General Meeting, 2006, pp. 1 pp.–. doi:10.1109/PES.2006.1709006.

[24] T. Mason, J. Millichamp, T. Neville, P. Shearing, S. Simons, D. Brett, A study of the effect of water management and electrode flooding on the dimensional change of polymer electrolyte fuel cells, Journal of Power Sources 242 (2013) 70 – 77. doi:http://dx.doi.org/10.1016/j.jpowsour.2013.05.045.

[25] H. Voss, D. Wilkinson, P. Pickup, M. Johnson, V. Basura, Anode water removal: A water management and diagnostic technique for solid polymer fuel cells, Electrochimica Acta 40 (3) (1995) 321 – 328. doi:http://dx.doi.org/10.1016/0013-4686(94)00266-4.

[26] M. Knobbe, W. He, P. Chong, T. Nguyen, Active gas management for PEM fuel cell stacks, Journal of Power Sources 138 (1?2) (2004) 94 – 100. doi:http://dx.doi.org/10.1016/j.jpowsour.2004.06.029.

[27] J. S.-P. et al., PEM fuel cells, in: Proceedings of the Second International Symposium on New Materials for Fuel Cell and Modern Battery Systems, 1997.

[28] A. Appleby, S. Gamburzev, Electroconductive fuel cell component with directly bonded layers and method for making same, wO Patent App. PCT/US2001/004,485 (Aug. 16 2001).
URL https://www.google.ch/patents/WO2001059862A2?cl=en

[29] N. Fletcher, C. Chow, E. Pow, B. Wozniczka, H. Voss, G. Hornburg, Electrochemical fuel cell stack with concurrently flowing coolant and oxidant streams, uS Patent 5,547,776 (Aug. 20 1996).
URL http://www.google.ch/patents/US5547776

[30] G. Karimi et al., Along-channel flooding prediction of polymer electrolyte membrane fuel cells, International Journal of Energy Research 35 (10) (2011) 883–896.

[31] Z. Wang, C. Wang, K. Chen, Two-phase flow and transport in the air cathode of proton exchange membrane fuel cells, Journal of Power Sources

94 (1) (2001) 40 – 50. doi:https://doi.org/10.1016/S0378-7753(00)00662-5.

[32] C. Bordons, A. Arce, A. J. del Real, Constrained predictive control strategies for pem fuel cells, in: 2006 American Control Conference, 2006, pp. 6 pp.–. doi:10.1109/ACC.2006.1656595.

[33] D. Chen, H. Peng, Modeling and simulation of a pem fuel cell humidification system, in: Proceedings of the 2004 American Control Conference, Vol. 1, 2004, pp. 822–827 vol.1.

[34] J. S. Yi, J. D. Yang, C. King, Water management along the flow channels of PEM fuel cells, AIChE Journal 50 (10) (2004) 2594–2603. doi:10.1002/aic.10307.
URL http://dx.doi.org/10.1002/aic.10307

[35] J. Huson, P. C. Lundberg, R. Herry, A. Bourgeau, A. Snyder, S. K. Das, E. U. Ubong, Experimental evaluation of the effect of humidification on the performaance of pem fuel cell stack, in: 2007 Electrical Insulation Conference and Electrical Manufacturing Expo, 2007, pp. 418–422. doi:10.1109/EEIC.2007.4562653.

[36] W. H. Hogarth, J. B. Benziger, Operation of polymer electrolyte membrane fuel cells with dry feeds: Design and operating strategies, Journal of Power Sources 159 (2) (2006) 968 – 978. doi:http://dx.doi.org/10.1016/j.jpowsour.2005.11.079.

[37] R. Methekar, V. Prasad, R. Gudi, Dynamic analysis and linear control strategies for proton exchange membrane fuel cell using a distributed parameter model, Journal of Power Sources 165 (1) (2007) 152–170.

[38] F. Chen, H.-S. Chu, C.-Y. Soong, W.-M. Yan, Effective schemes to control the dynamic behavior of the water transport in the membrane of PEM fuel cell, Journal of Power Sources 140 (2) (2005) 243 – 249. doi:http://dx.doi.org/10.1016/j.jpowsour.2004.08.026.

[39] A. Miotti, A. D. Domenico, Y. G. Guezennec, S. Rajagopalan, Control-oriented model for an automotive PEM fuel cell system with imbedded 1+1d membrane water transport, in: 2005 IEEE Vehicle Power and Propulsion Conference, 2005, pp. 8 pp.–. doi:10.1109/VPPC.2005.1554622.

[40] B. A. McCain, A. G. Stefanopoulou, I. V. Kolmanovsky, A multi-component spatially-distributed model of two-phase flow for estimation and control of fuel cell water dynamics, in: 2007 46th IEEE Conference on Decision and Control, 2007, pp. 584–589. doi:10.1109/CDC.2007.4434923.

[41] W. Garcia-Gabin, F. Dorado, C. Bordons, Real-time implementation of a sliding mode controller for air supply on a pem fuel cell, Journal of Process Control 20 (3) (2010) 325 – 336. doi:http://dx.doi.org/10.1016/j.jprocont.2009.11.006.

[42] M. Mangold, A. Bück, R. Hanke-Rauschenbach, Passivity based control of a distributed pem fuel cell model, Journal of Process Control 20 (3) (2010) 292–313.

[43] M. Sarmiento-Carnevali, M. Serra, C. Batlle, Distributed parameter model simulation tool for PEM fuel cells, International Journal of Hydrogen Energy 39 (8) (2014) 4044 – 4052. doi:http://dx.doi.org/10.1016/j.ijhydene.2013.04.015.

[44] T. E. Springer, T. A. Zawodzinski, S. Gottesfeld, Polymer electrolyte fuel cell model, Journal of The Electrochemical Society 138 (8) (1991) 2334–2342. doi:10.1149/1.2085971.

[45] P. K. Kundu, I. M. Cohen, Fluid Mechanics, Academic Press, 1990.

[46] J. M. Sergi, S. G. Kandlikar, Quantification and characterization of water coverage in pemfc gas channels using simultaneous anode and cathode visualization and image processing, International Journal of Hydrogen Energy 36 (19) (2011) 12381–12392. doi:10.1016/j.ijhydene.2011.06.092.

[47] F. Barbir, PEM Fuel Cells: Theory and Practice, Academic Press, 2005.

[48] E. Camacho, C. Bordons, Model Predictive Control, Springer, 2012.

[49] B. Moore, Principal component analysis in linear systems: Controllability, observability, and model reduction, Automatic Control, IEEE Transactions on 26 (1) (1981) 17–32.

[50] A. C. Antoulas, Lectures on the approximation of large-scale dynamical systems, in: SIAM Press, 2002.

[51] C. Batlle, N. Roqueiro, Balanced model order reduction for systems depending on a parameter, CoRR abs/1604.08086 (2016) 1–14.
URL https://arxiv.org/abs/1604.08086

[52] K. Ogata, Modern Control Engineering, Pearson, 2005.

[53] Vauxhall, U. Kingdom, WLTP driving cycle (2017).
URL http://www.vauxhall.co.uk/discover-vauxhall/technology/wltp.html

[54] F. Migliardini, T. D. Palma, M. Gaele, P. Corbo, Hydrogen purge and reactant feeding strategies in self-humidified PEM fuel cell systems, International Journal of Hydrogen Energy 42 (3) (2017) 1758 – 1765.

[55] A. Su, F. Weng, C. Hsu, Y. Chen, Studies on flooding in PEM fuel cell cathode channels, International Journal of Hydrogen Energy 31 (8) (2006) 1031 – 1039, fuel CellsFuel Cells. doi:http://dx.doi.org/10.1016/j.ijhydene.2005.12.019.

[56] S. Ge, C. Wang, Cyclic voltammetry study of ice formation in the PEFC catalyst layer during cold start, Journal of The Electrochemical Society 154 (12) (2007) B1399–B1406. doi:10.1149/1.2784166.

[57] U. Pasaogullari, C. Wang, Two-phase modeling and flooding prediction of polymer electrolyte fuel cells, Journal of The Electrochemical Society 152 (2) (2005) A380–A390. doi:10.1149/1.1850339.

Figure 1

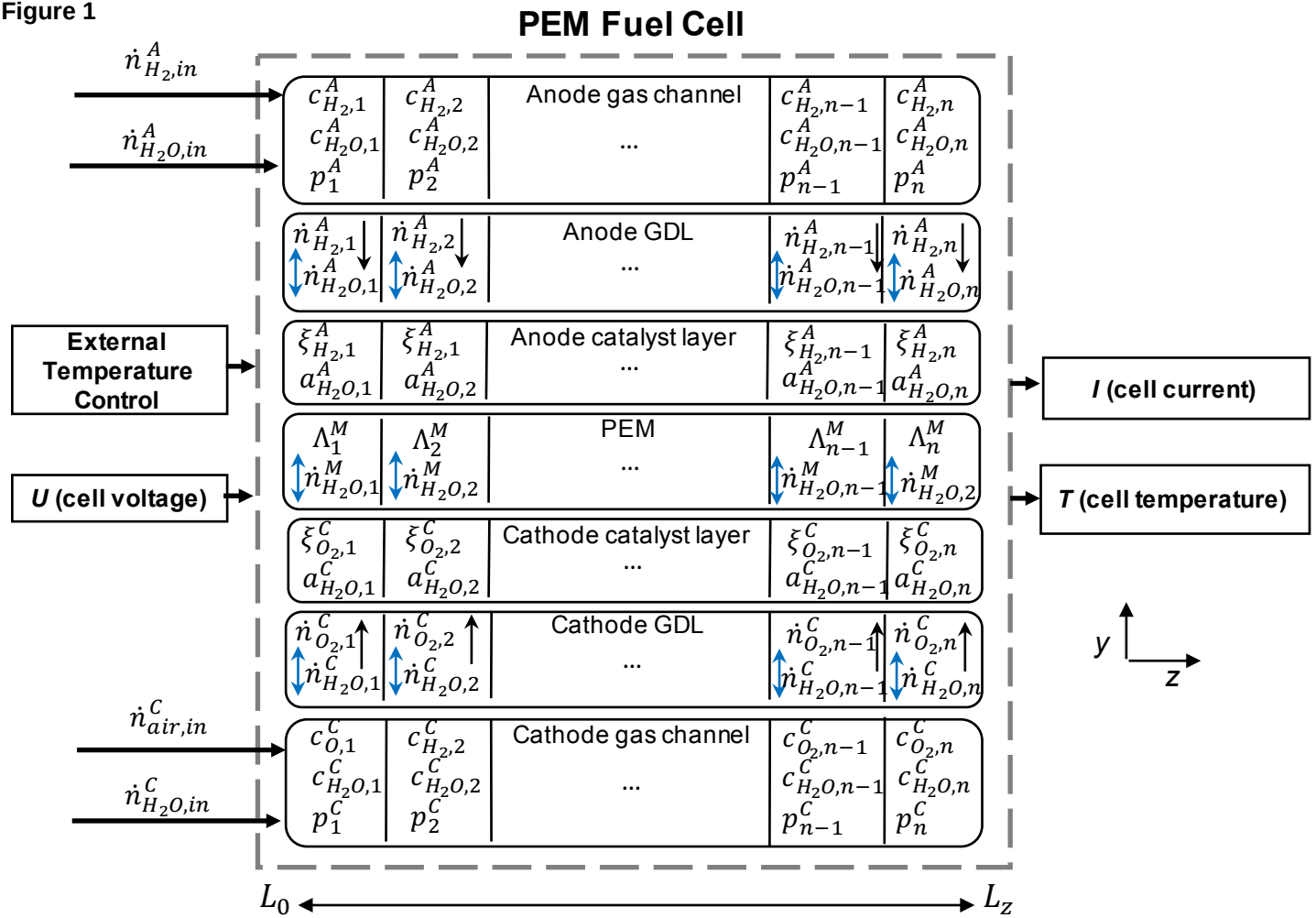
PEM Fuel Cell
$\dot{n}^A_{H_2,in}$
$\dot{n}^A_{H_2O,in}$
Anode gas channel
$c^A_{H_2,1}$ $c^A_{H_2,2}$ ... $c^A_{H_2,n-1}$ $c^A_{H_2,n}$
$c^A_{H_2O,1}$ $c^A_{H_2O,2}$ $c^A_{H_2O,n-1}$ $c^A_{H_2O,n}$
p^A_1 p^A_2 p^A_{n-1} p^A_n
Anode GDL
$\dot{n}^A_{H_2,1}$ $\dot{n}^A_{H_2,2}$ $\dot{n}^A_{H_2,n-1}$ $\dot{n}^A_{H_2,n}$
$\dot{n}^A_{H_2O,1}$ $\dot{n}^A_{H_2O,2}$ $\dot{n}^A_{H_2O,n-1}$ $\dot{n}^A_{H_2O,n}$
Anode catalyst layer
$\xi^A_{H_2,1}$ $\xi^A_{H_2,1}$ $\xi^A_{H_2,n-1}$ $\xi^A_{H_2,n}$
$a^A_{H_2O,1}$ $a^A_{H_2O,2}$ $a^A_{H_2O,n-1}$ $a^A_{H_2O,n}$
PEM
Λ^M_1 Λ^M_2 Λ^M_{n-1} Λ^M_n
$\dot{n}^M_{H_2O,1}$ $\dot{n}^M_{H_2O,2}$ $\dot{n}^M_{H_2O,n-1}$ $\dot{n}^M_{H_2O,2}$
Cathode catalyst layer
$\xi^C_{O_2,1}$ $\xi^C_{O_2,2}$ $\xi^C_{O_2,n-1}$ $\xi^C_{O_2,n}$
$a^C_{H_2O,1}$ $a^C_{H_2O,2}$ $a^C_{H_2O,n-1}$ $a^C_{H_2O,n}$
Cathode GDL
$\dot{n}^C_{O_2,1}$ $\dot{n}^C_{O_2,2}$ $\dot{n}^C_{O_2,n-1}$ $\dot{n}^C_{O_2,n}$
$\dot{n}^C_{H_2O,1}$ $\dot{n}^C_{H_2O,2}$ $\dot{n}^C_{H_2O,n-1}$ $\dot{n}^C_{H_2O,n}$
Cathode gas channel
$c^C_{O,1}$ $c^C_{H_2,2}$ $c^C_{O_2,n-1}$ $c^C_{O_2,n}$
$c^C_{H_2O,1}$ $c^C_{H_2O,2}$ $c^C_{H_2O,n-1}$ $c^C_{H_2O,n}$
p^C_1 p^C_2 p^C_{n-1} p^C_n
$\dot{n}^C_{air,in}$
$\dot{n}^C_{H_2O,in}$
External Temperature Control
U (cell voltage)
I (cell current)
T (cell temperature)
y
z
L_0
L_z

Figure 2

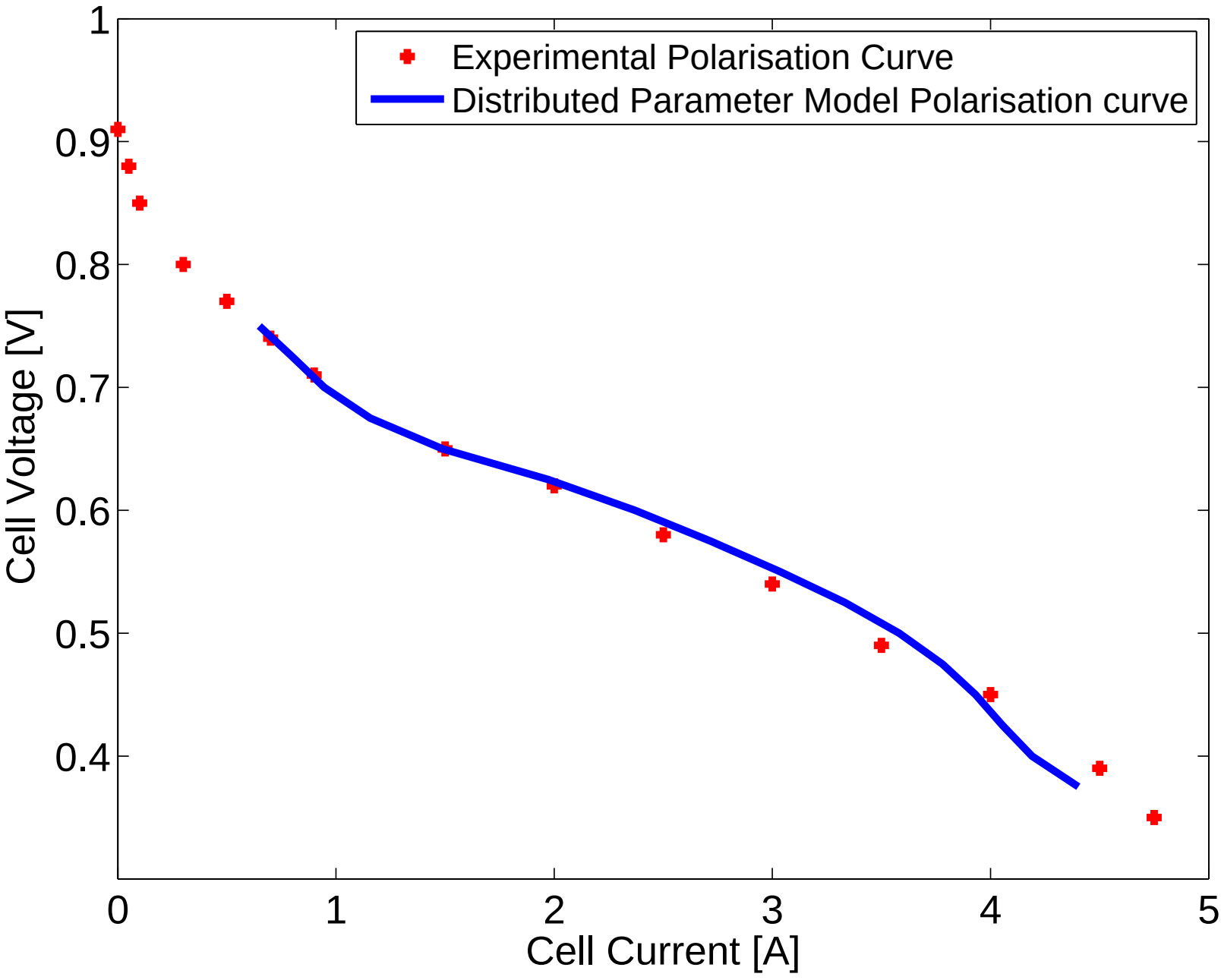
Experimental Polarisation Curve
Distributed Parameter Model Polarisation curve
Cell Voltage [V]
Cell Current [A]
1
0.9
0.8
0.7
0.6
0.5
0.4
0
1
2
3
4
5

Figure 3

Click here to download high resolution image

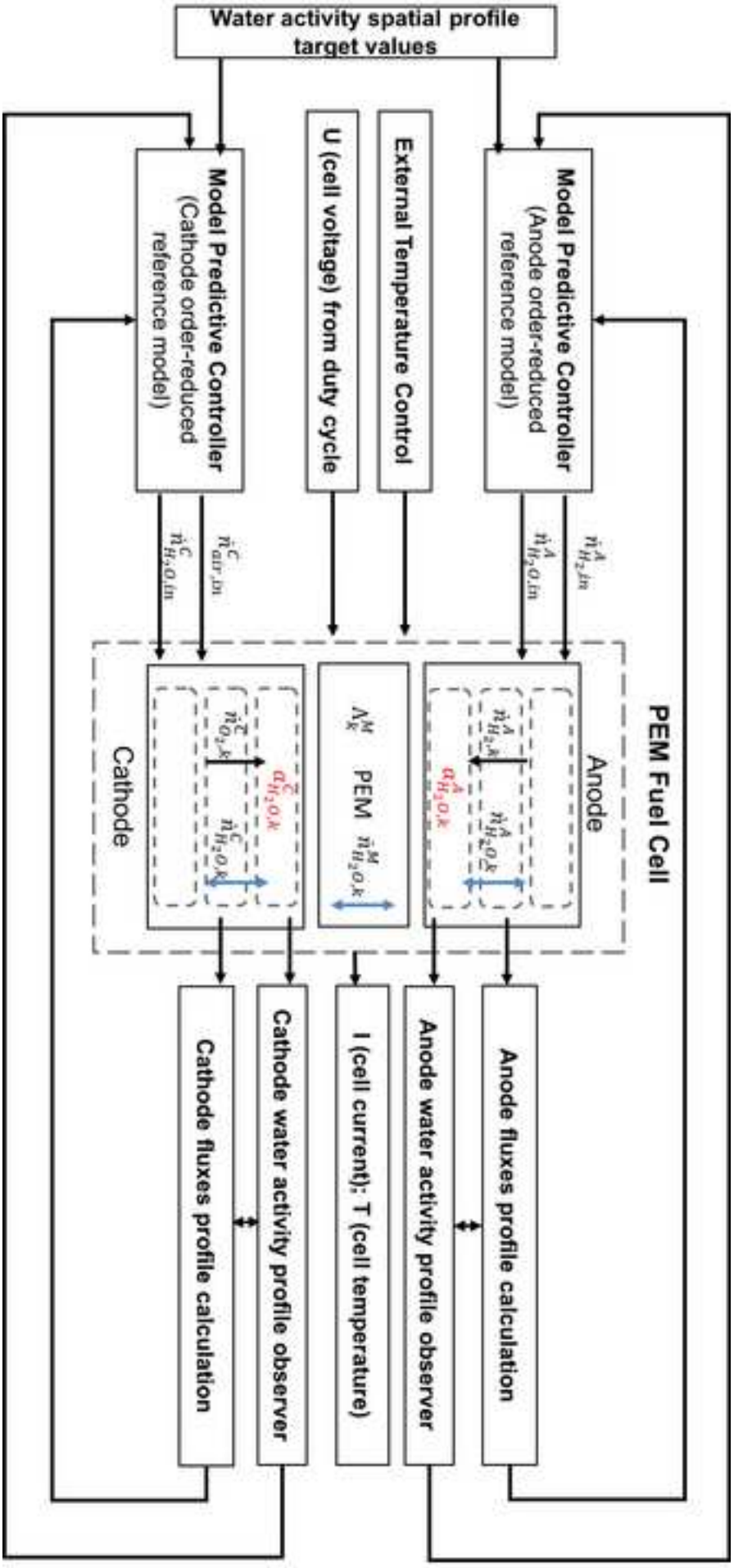

Figure 4a

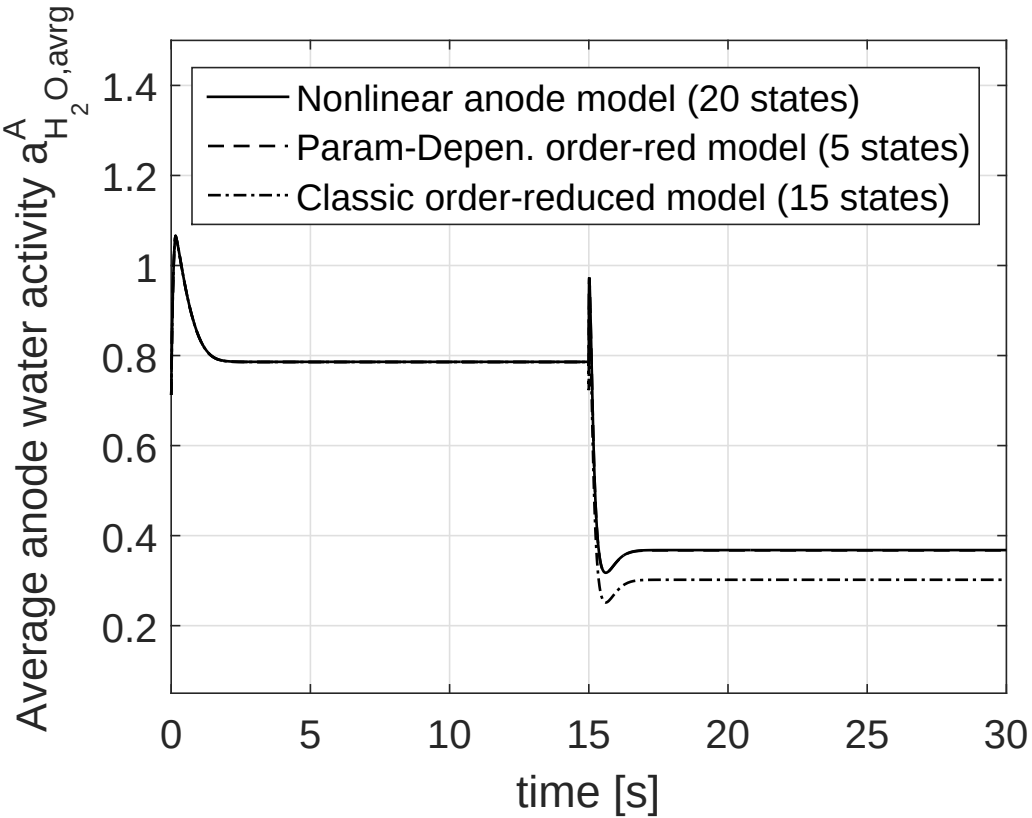
Nonlinear anode model (20 states)
Param-Depen. order-red model (5 states)
Classic order-reduced model (15 states)
Average anode water activity $a^{A}_{H_2O,avrg}$
time [s]
0
5
10
15
20
25
30
0.2
0.4
0.6
0.8
1
1.2
1.4

Figure 4b

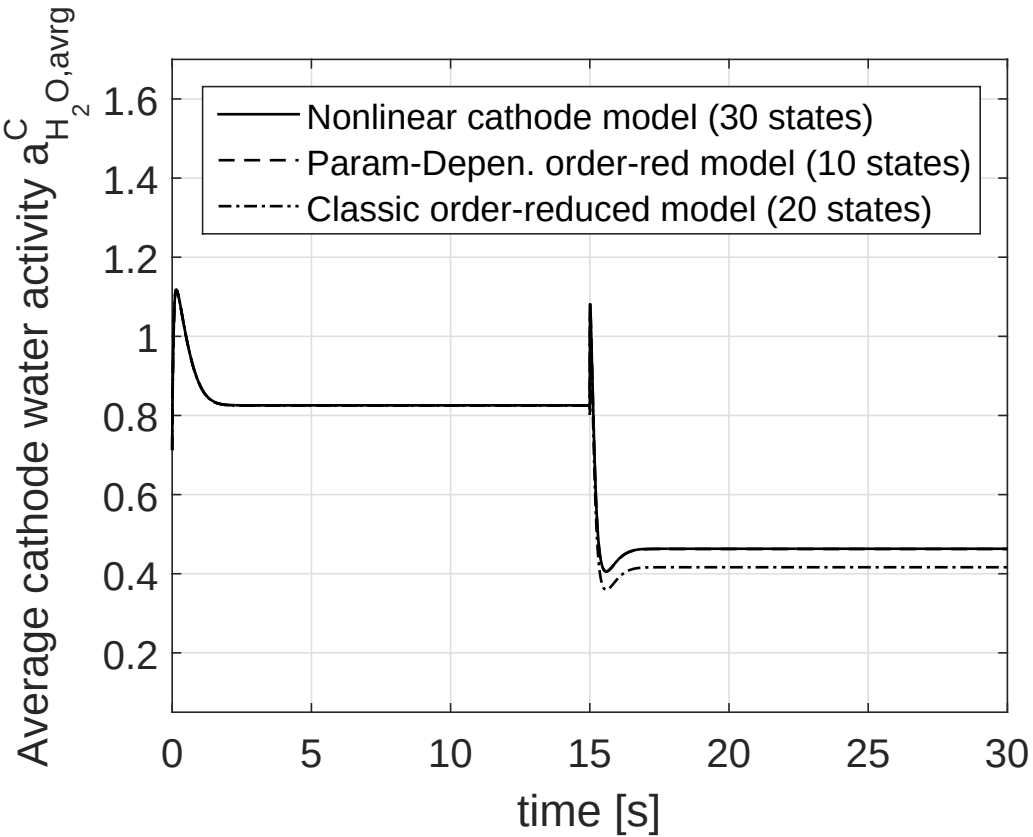
Nonlinear cathode model (30 states)
Param-Depen. order-red model (10 states)
Classic order-reduced model (20 states)
Average cathode water activity $a^{C}_{H_2O,avrg}$
time [s]
0.2
0.4
0.6
0.8
1
1.2
1.4
1.6
0
5
10
15
20
25
30

Figure 5a

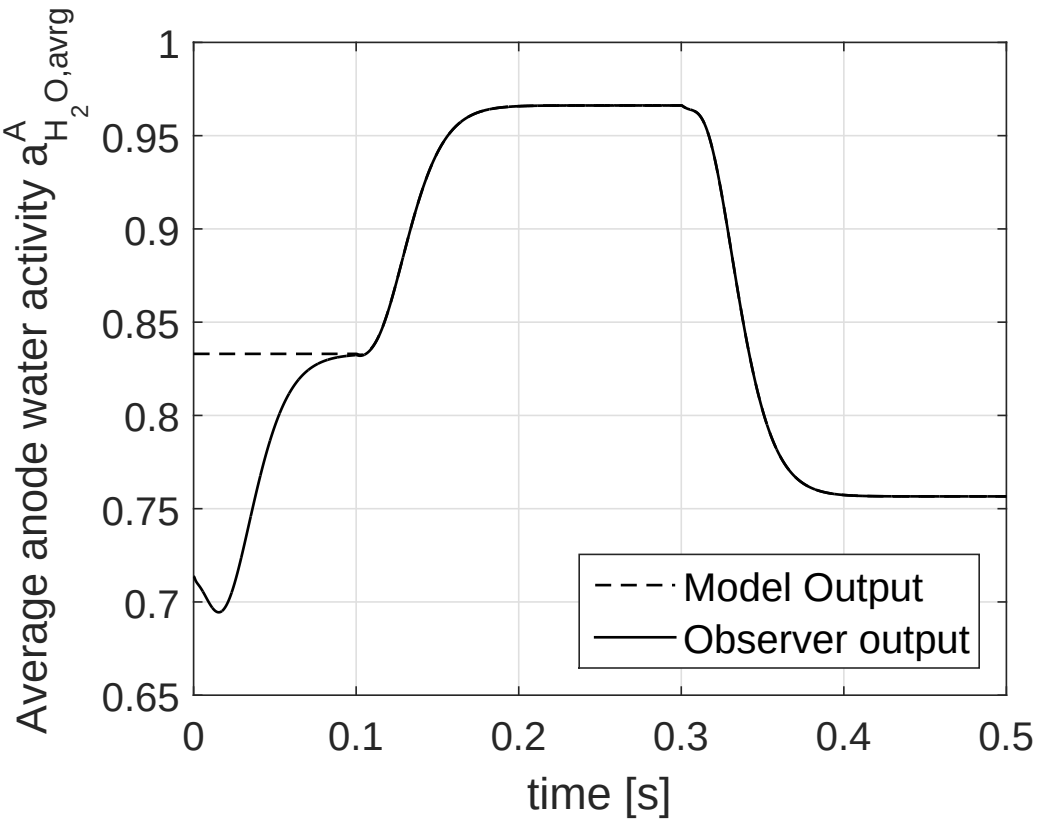
Average anode water activity $a^{A}_{H_2O,avrg}$
1
0.95
0.9
0.85
0.8
0.75
0.7
0.65
0
0.1
0.2
0.3
0.4
0.5
time [s]
Model Output
Observer output

Figure 5b

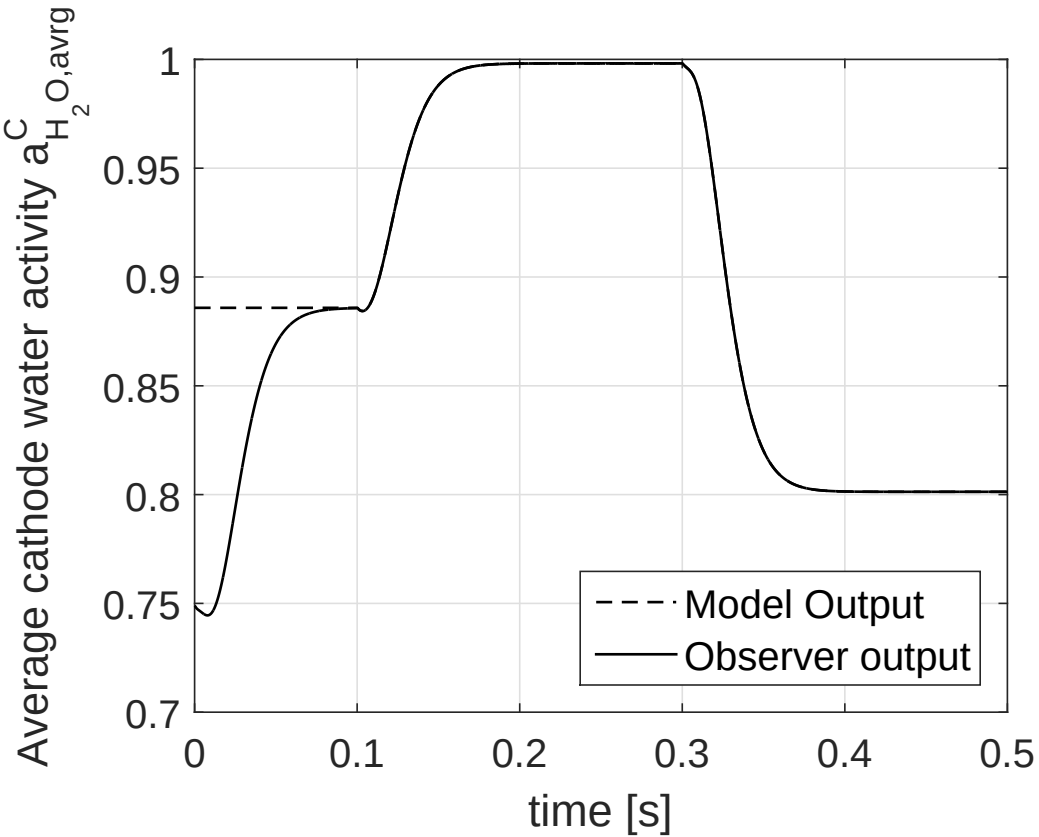
Average cathode water activity $a^{C}_{H_2O,avrg}$
1
0.95
0.9
0.85
0.8
0.75
0.7
0
0.1
0.2
0.3
0.4
0.5
time [s]
Model Output
Observer output

Figure 6a

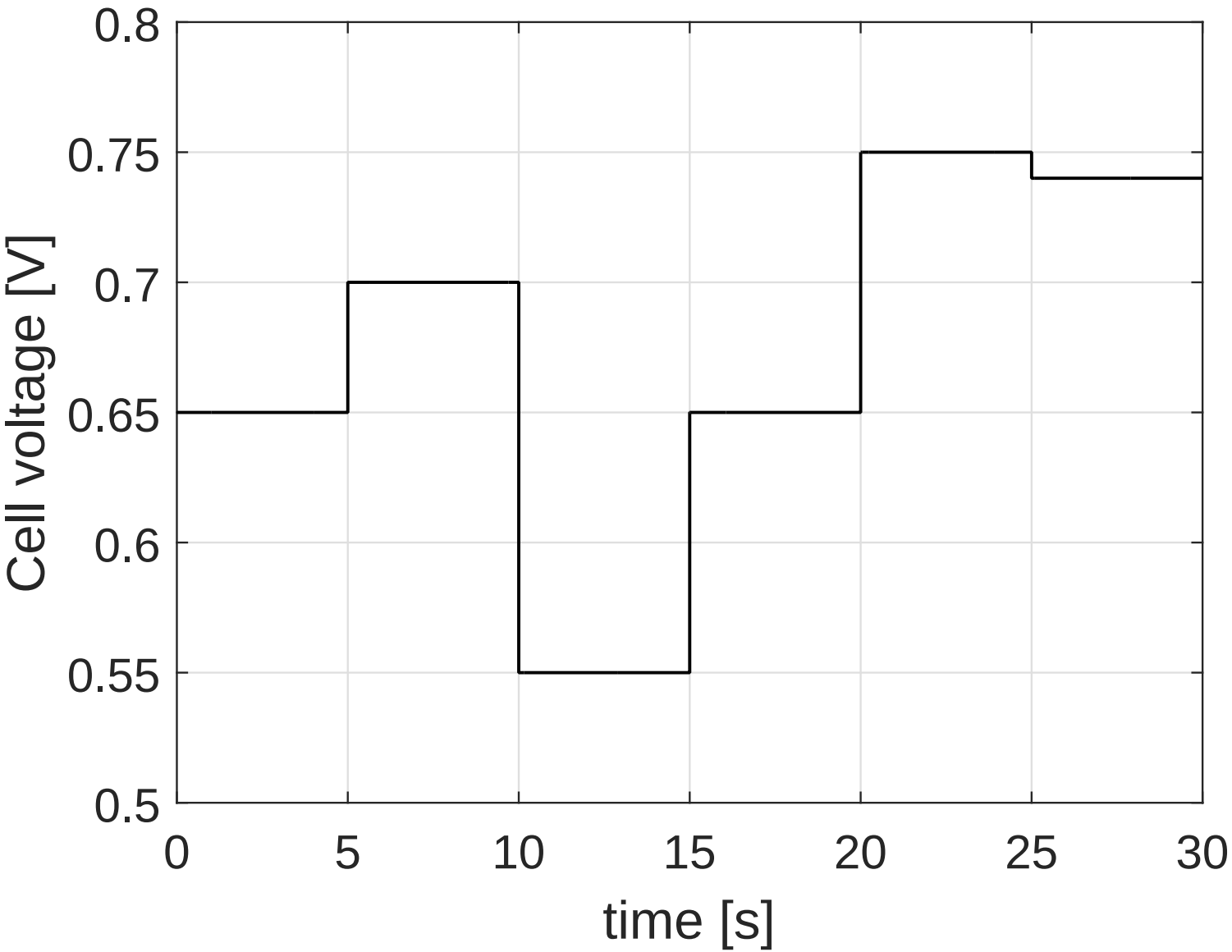

Figure 6b

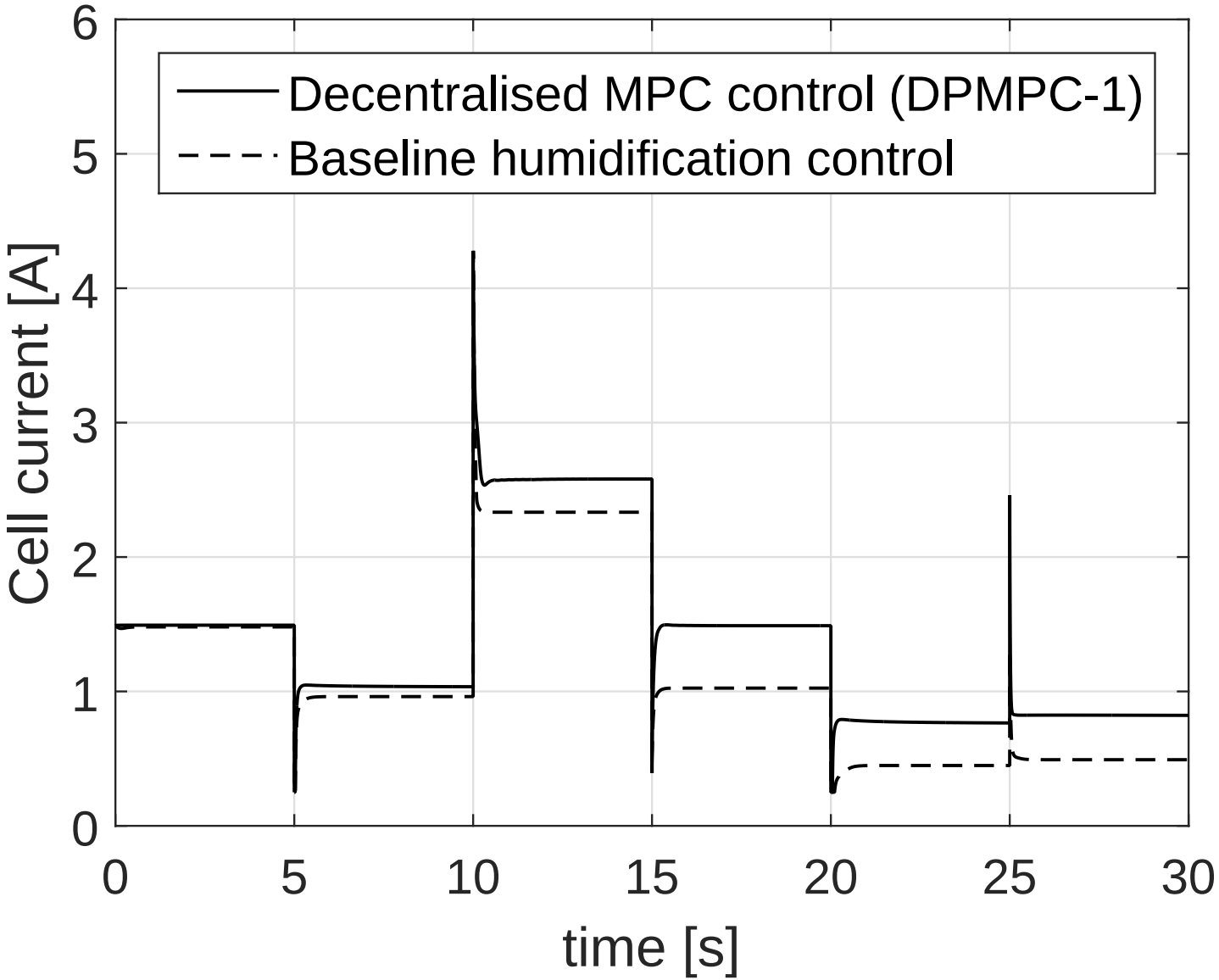
Decentralised MPC control (DPMPC-1)
Baseline humidification control
Cell current [A]
time [s]
0
1
2
3
4
5
6
0
5
10
15
20
25
30

Figure 6c

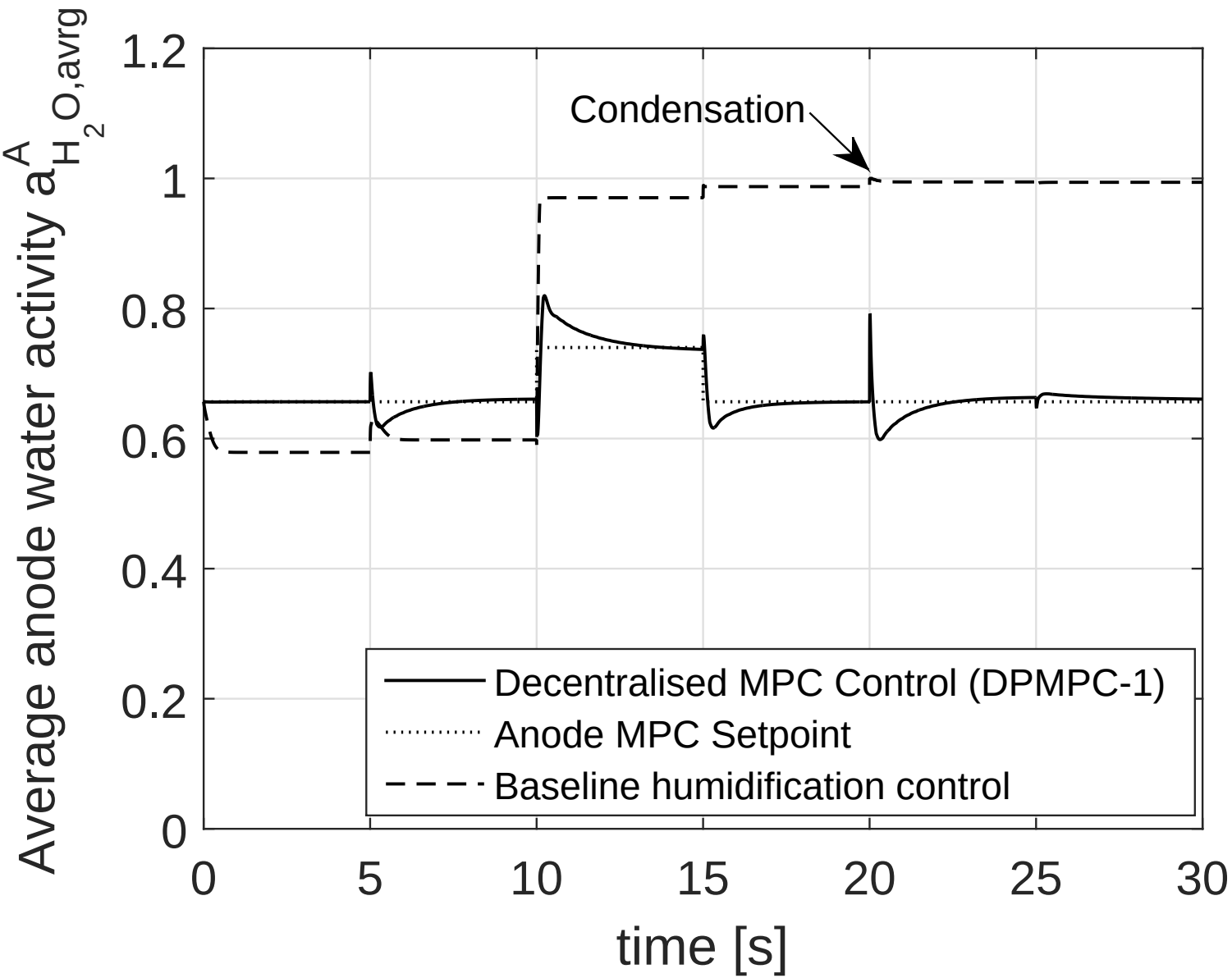
Average anode water activity $a^{A}_{H_2O,avrg}$
1.2
1
0.8
0.6
0.4
0.2
0
Condensation
Decentralised MPC Control (DPMPC-1)
Anode MPC Setpoint
Baseline humidification control
0
5
10
15
20
25
30
time [s]

Figure 6d

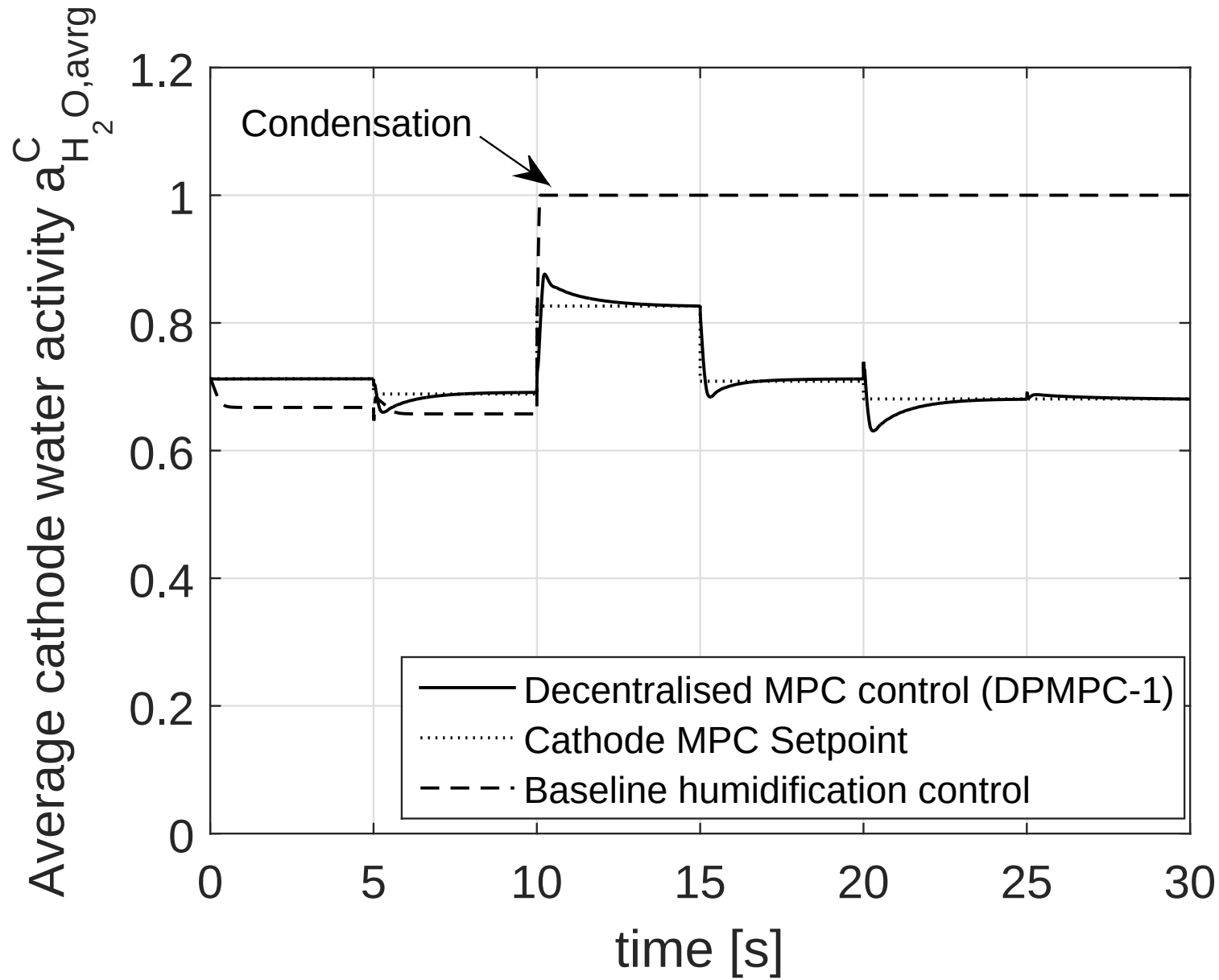
Average cathode water activity $a^{C}_{H_2O,avrg}$
1.2
1
0.8
0.6
0.4
0.2
0
Condensation
0
5
10
15
20
25
30
time [s]
Decentralised MPC control (DPMPC-1)
Cathode MPC Setpoint
Baseline humidification control

Figure 6e

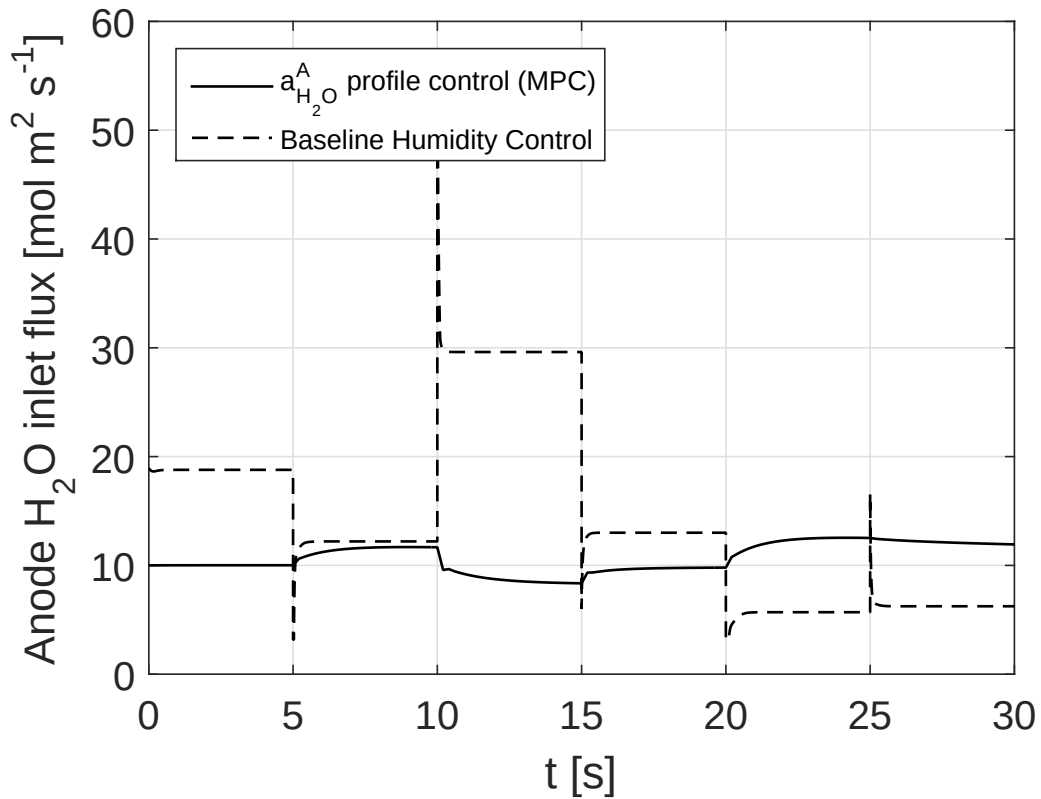
60
50
40
30
20
10
0
0
5
10
15
20
25
30
t [s]
Anode H2O inlet flux [mol m2 s-1]
a^A_H2O profile control (MPC)
Baseline Humidity Control

Figure 6f

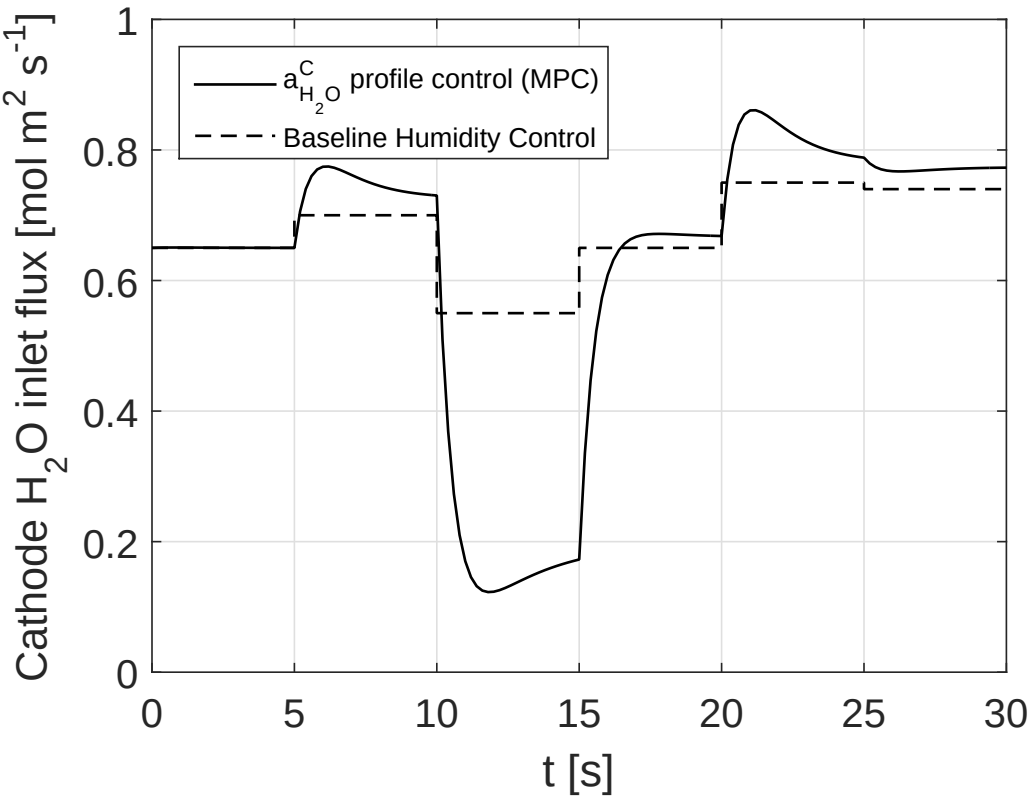
1
0.8
0.6
0.4
0.2
0
0
5
10
15
20
25
30
t [s]
Cathode H2O inlet flux [mol m2 s-1]
a C H2O profile control (MPC)
Baseline Humidity Control

Figure 7a

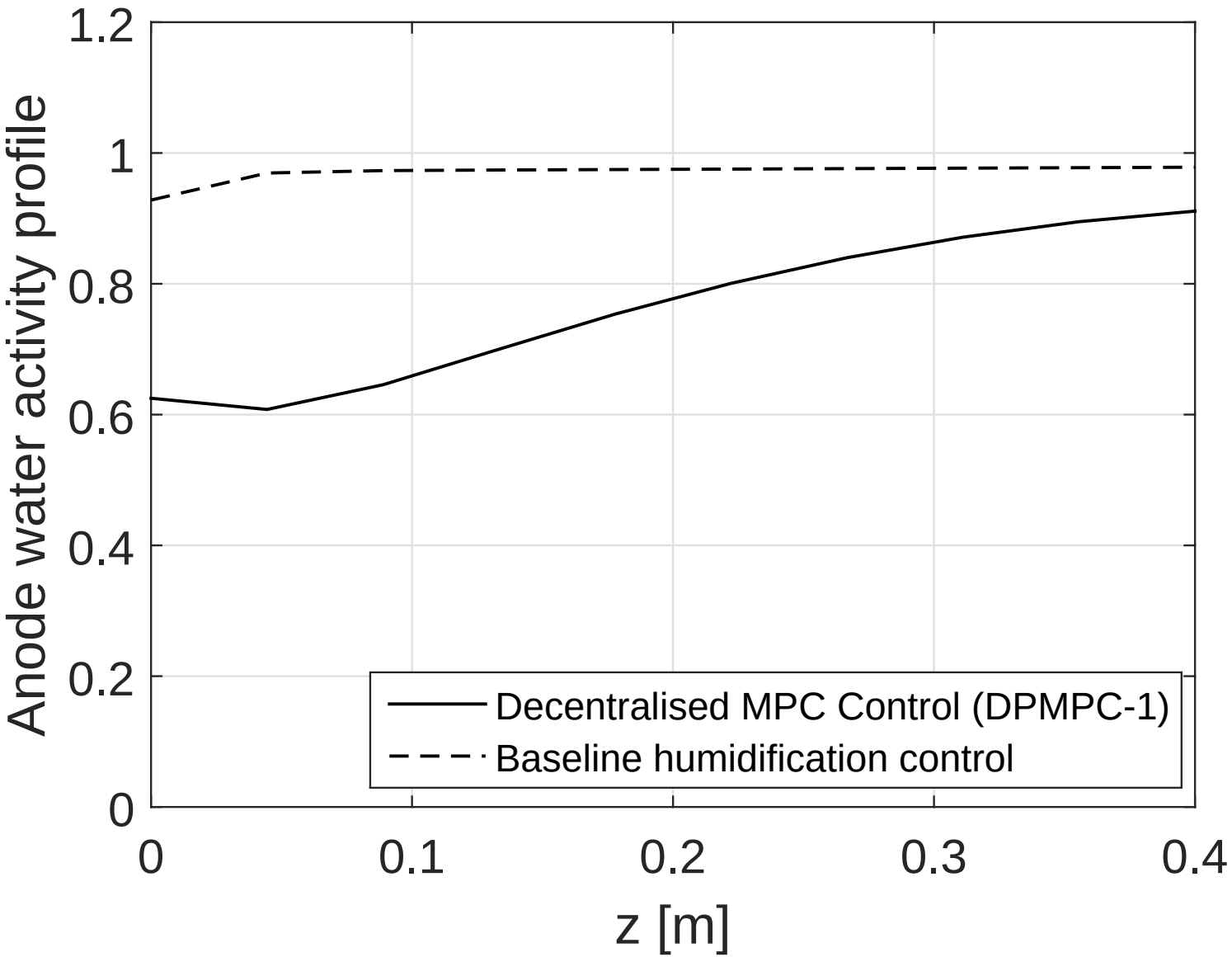
1.2
1
0.8
0.6
0.4
0.2
0
Anode water activity profile
0
0.1
0.2
0.3
0.4
z [m]
Decentralised MPC Control (DPMPC-1)
Baseline humidification control

Figure 7b

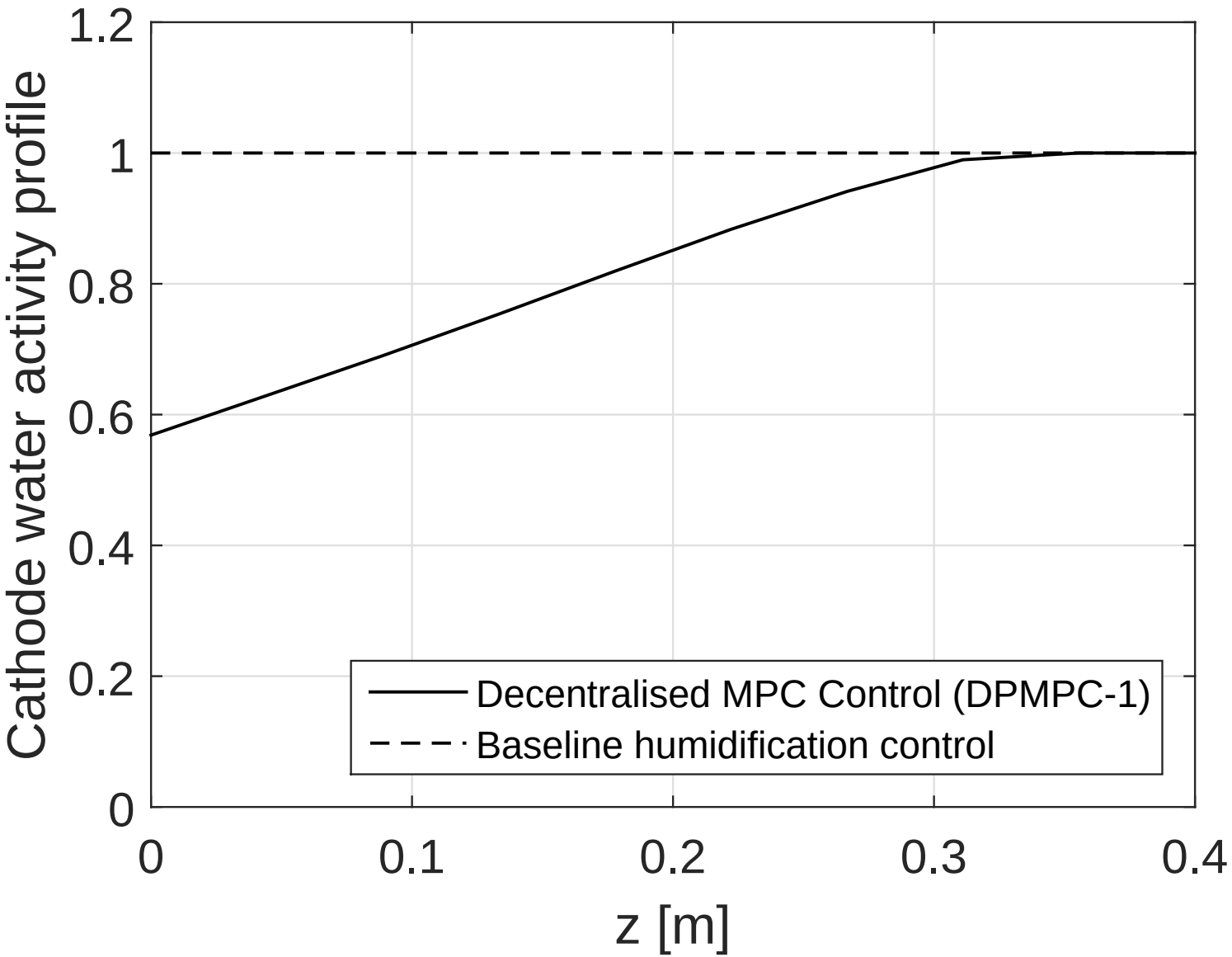
Cathode water activity profile
1.2
1
0.8
0.6
0.4
0.2
0
0
0.1
0.2
0.3
0.4
z [m]
Decentralised MPC Control (DPMPC-1)
Baseline humidification control

Figure 7c

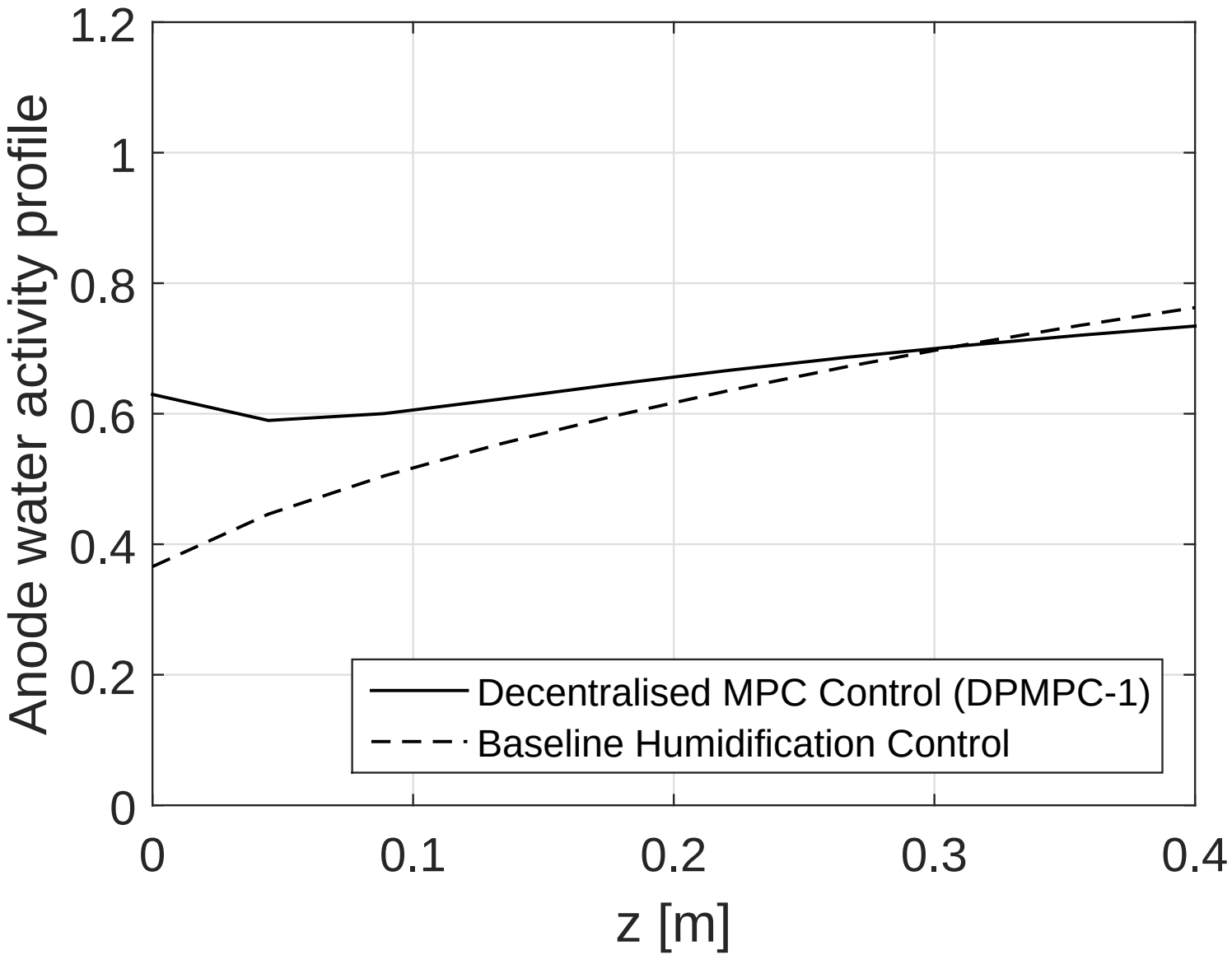
1.2
1
0.8
0.6
0.4
0.2
0
Anode water activity profile
0
0.1
0.2
0.3
0.4
z [m]
Decentralised MPC Control (DPMPC-1)
Baseline Humidification Control

Figure 7d

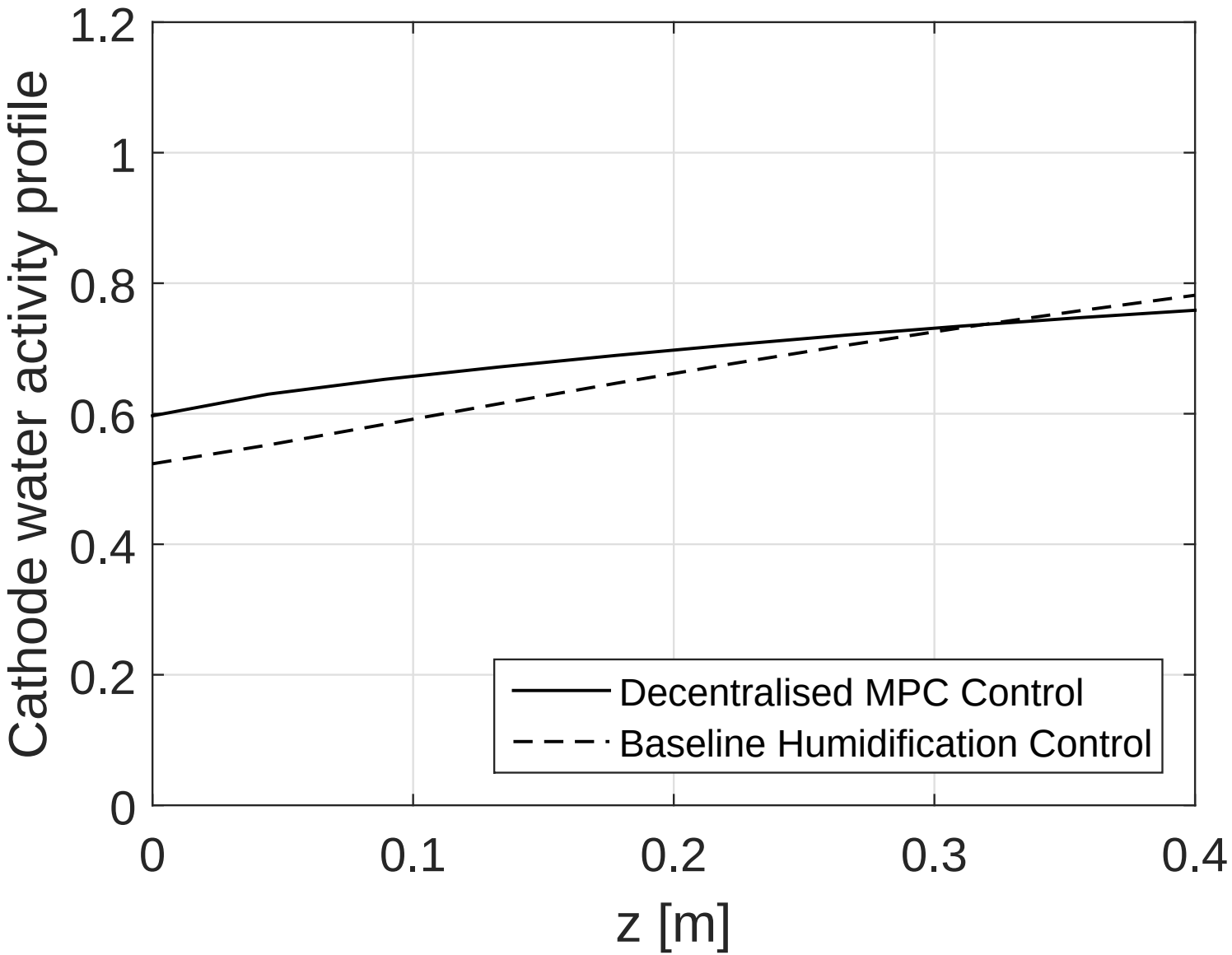
Cathode water activity profile
1.2
1
0.8
0.6
0.4
0.2
0
0
0.1
0.2
0.3
0.4
z [m]
Decentralised MPC Control
Baseline Humidification Control

Figure 7e

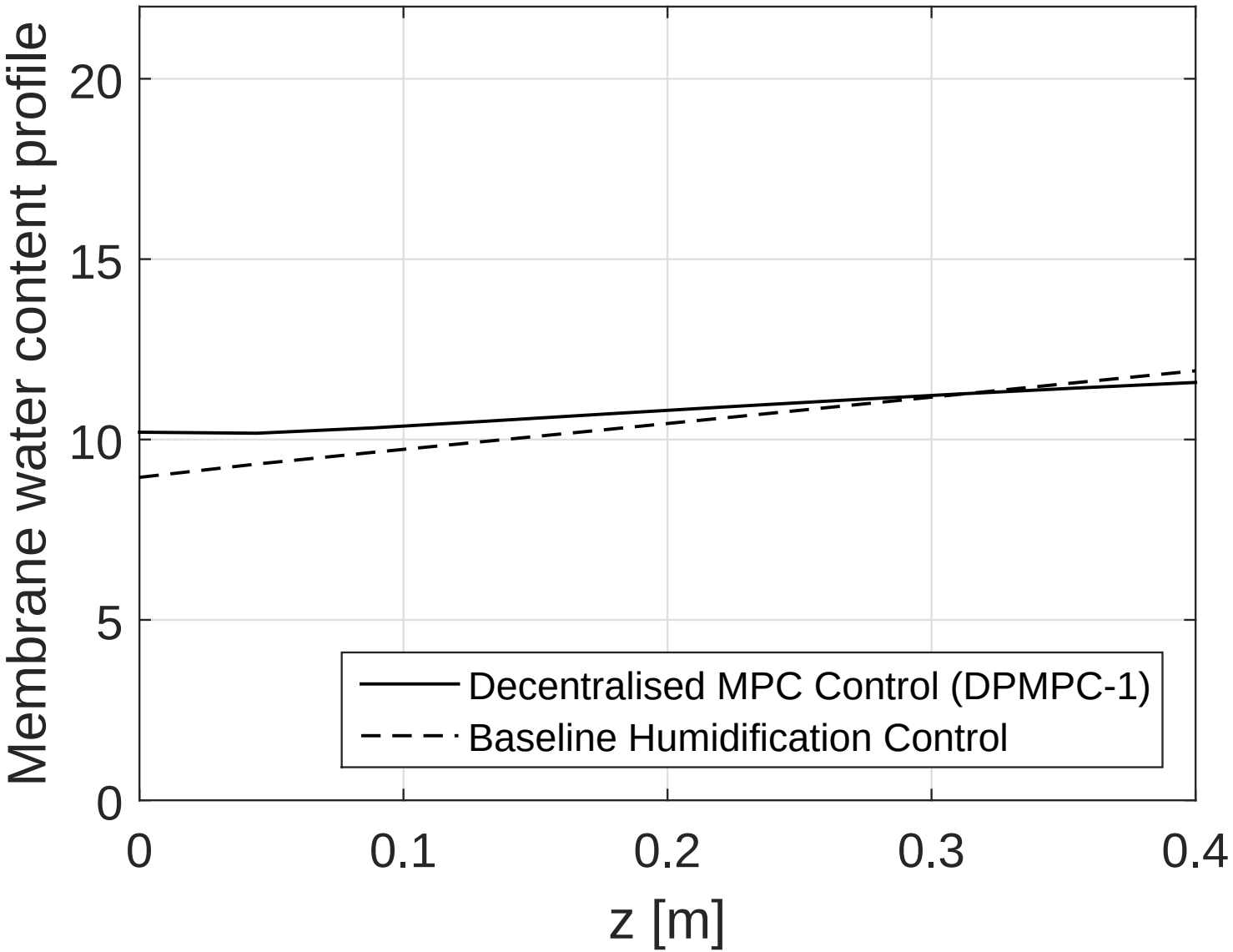
Membrane water content profile
20
15
10
5
0
0
0.1
0.2
0.3
0.4
z [m]
Decentralised MPC Control (DPMPC-1)
Baseline Humidification Control

Figure 7f

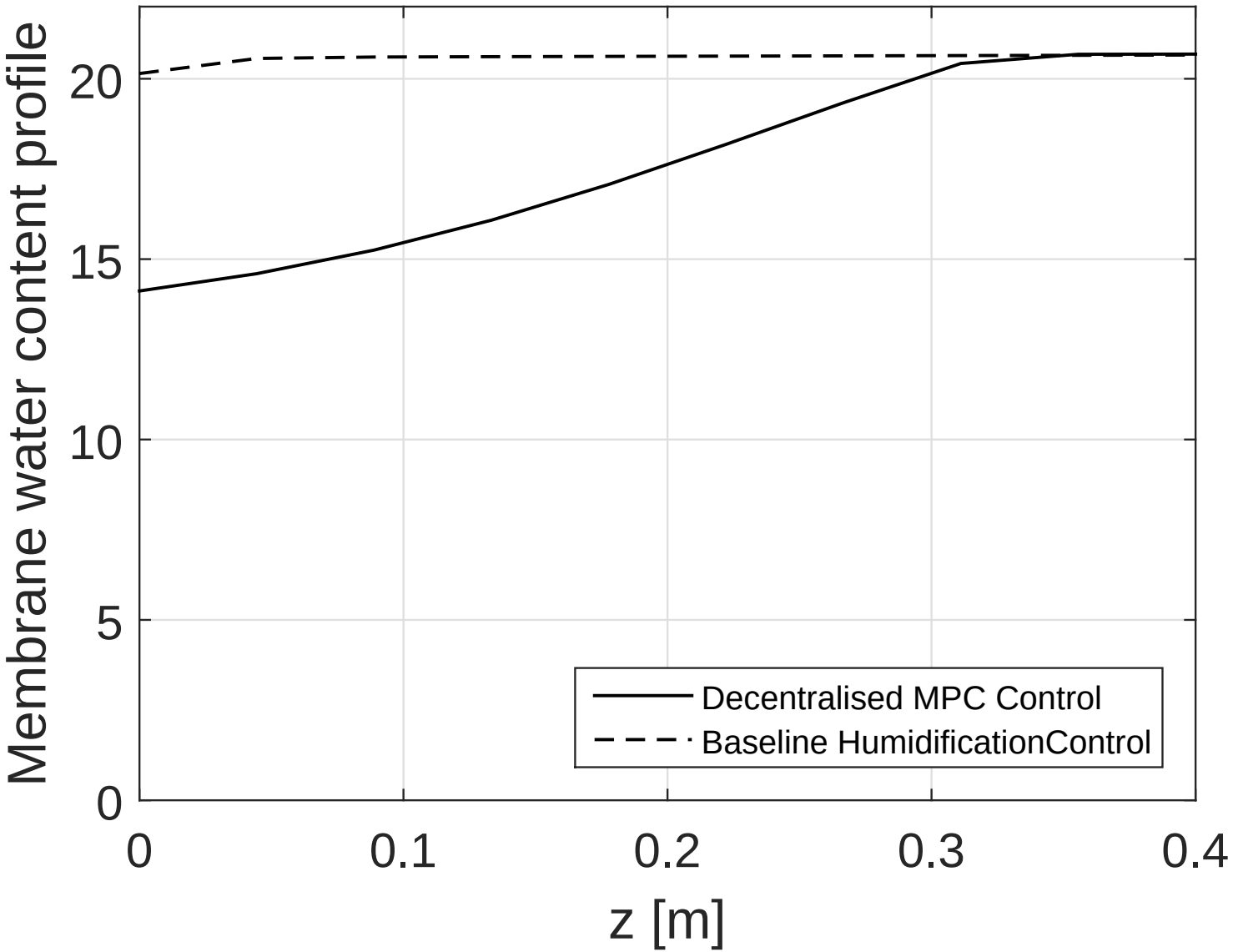
Membrane water content profile
20
15
10
5
0
0
0.1
0.2
0.3
0.4
z [m]
Decentralised MPC Control
Baseline HumidificationControl

Figure 8a

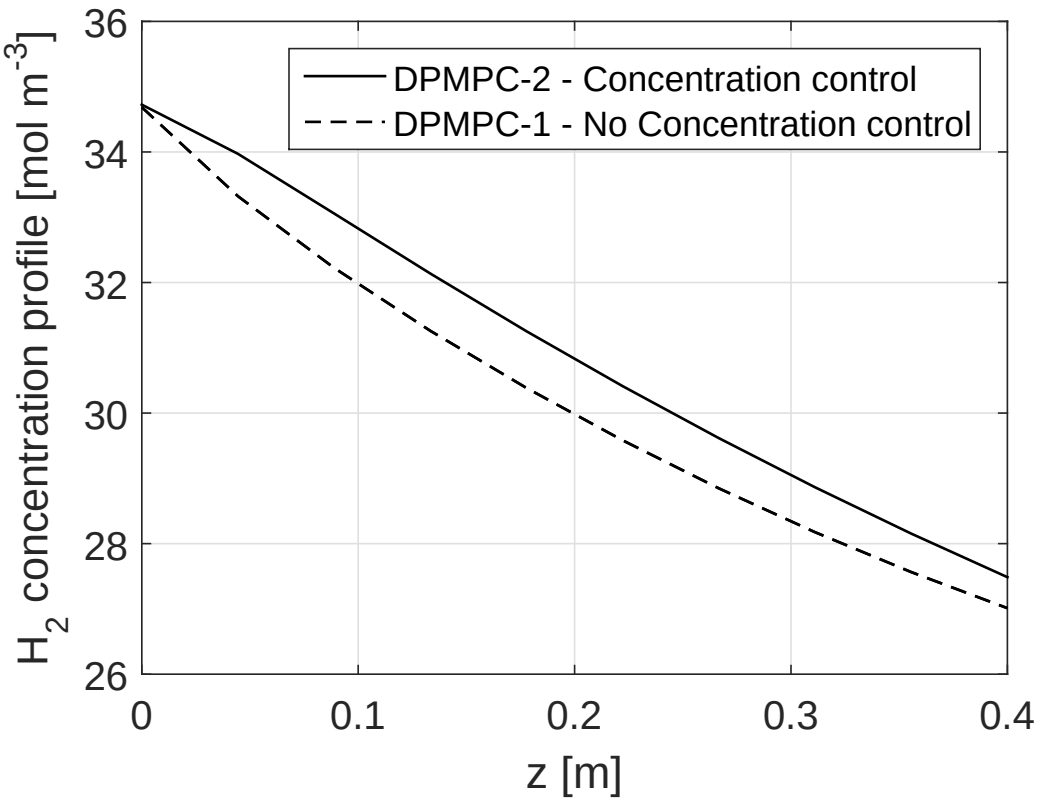
DPMPC-2 - Concentration control
DPMPC-1 - No Concentration control
H2 concentration profile [mol m-3]
z [m]
36
34
32
30
28
26
0
0.1
0.2
0.3
0.4

Figure 8b

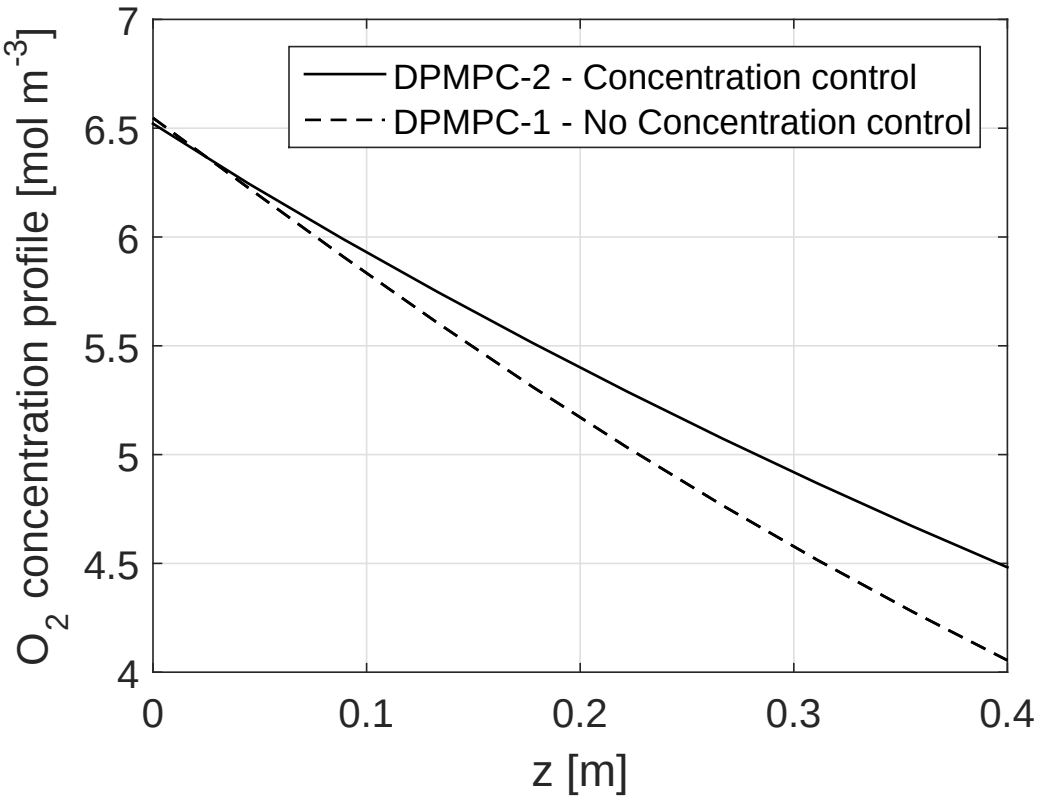
DPMPC-2 - Concentration control
DPMPC-1 - No Concentration control
O_2 concentration profile [mol m^{-3}]
z [m]
7
6.5
6
5.5
5
4.5
4
0
0.1
0.2
0.3
0.4

Figure 9a

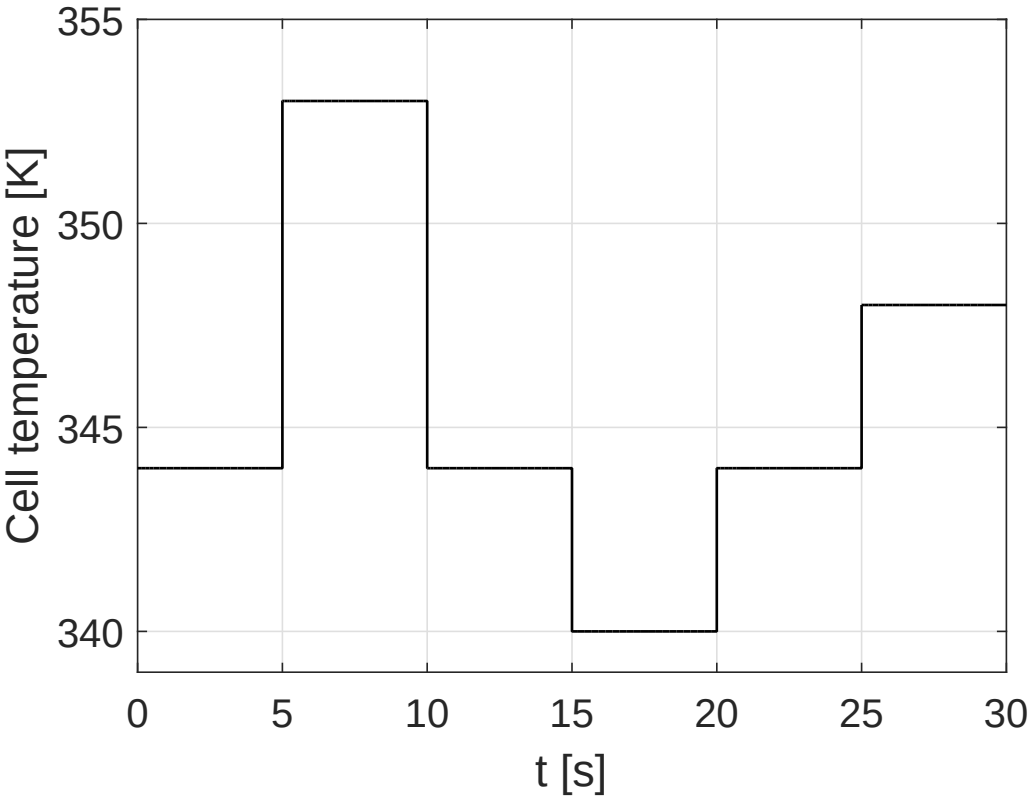

Figure 9b

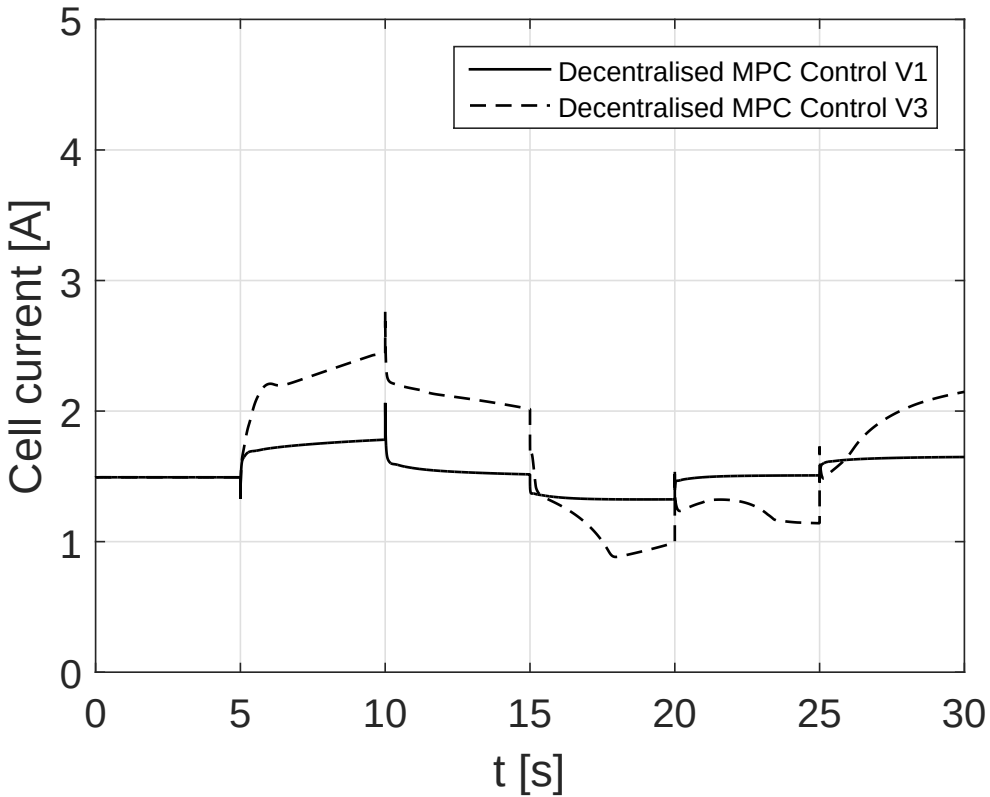
Decentralised MPC Control V1
Decentralised MPC Control V3
Cell current [A]
t [s]
0
1
2
3
4
5
0
5
10
15
20
25
30

Figure 9c

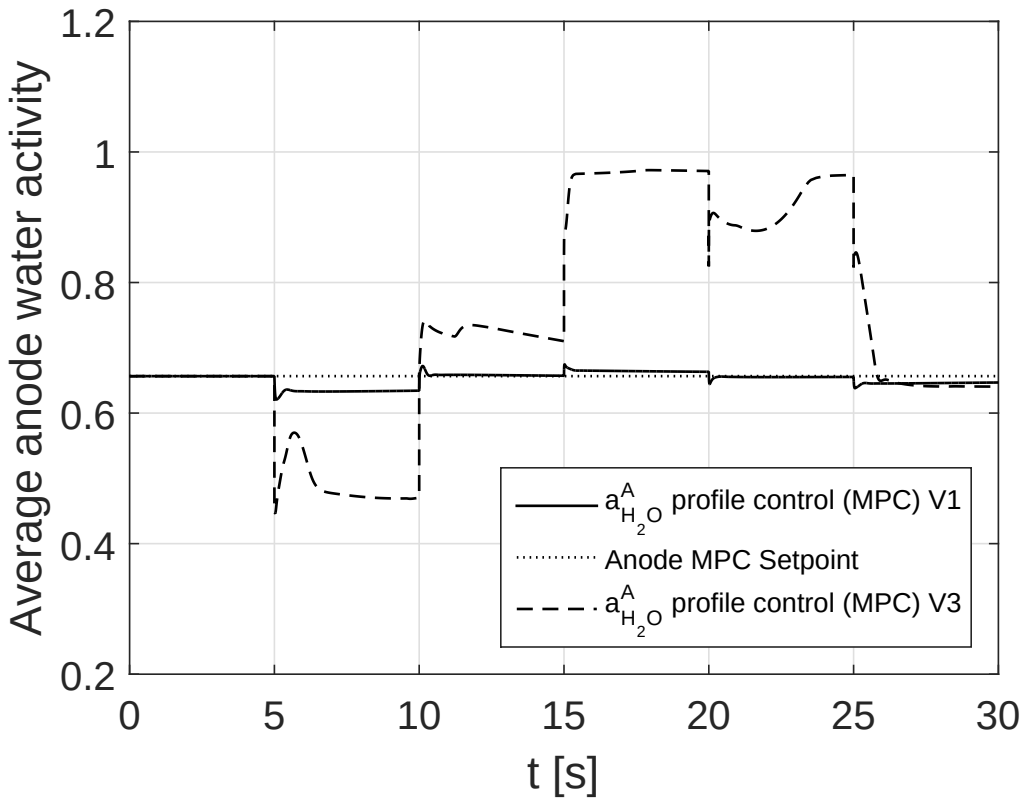
Average anode water activity
t [s]
1.2
1
0.8
0.6
0.4
0.2
0
5
10
15
20
25
30
$a^{A}_{H_2O}$ profile control (MPC) V1
Anode MPC Setpoint
$a^{A}_{H_2O}$ profile control (MPC) V3

Figure 9d

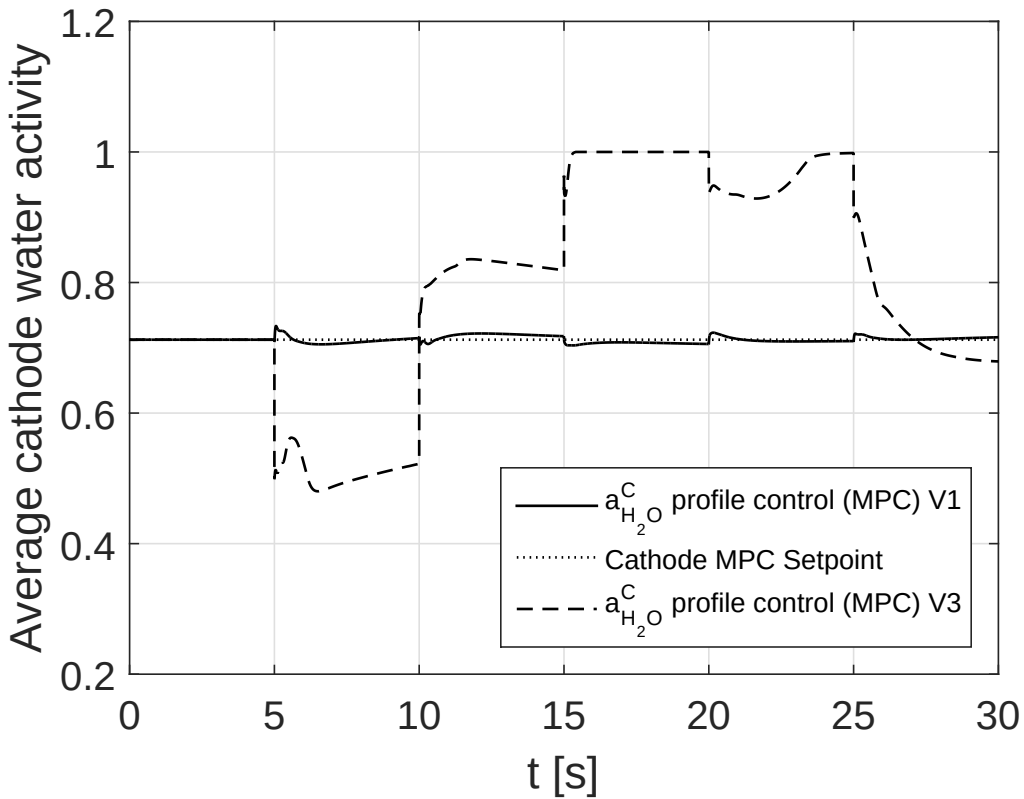
Average cathode water activity
t [s]
1.2
1
0.8
0.6
0.4
0.2
0
5
10
15
20
25
30
$a^{C}_{H_2O}$ profile control (MPC) V1
Cathode MPC Setpoint
$a^{C}_{H_2O}$ profile control (MPC) V3

Figure 9e

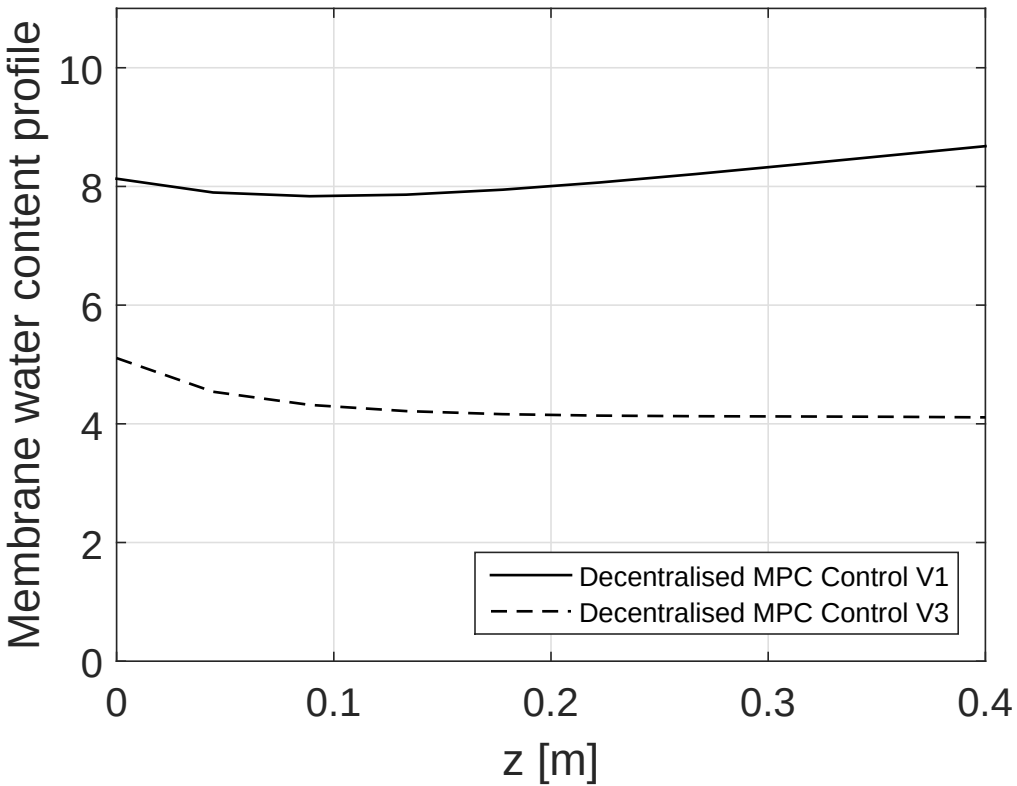
Membrane water content profile
10
8
6
4
2
0
0
0.1
0.2
0.3
0.4
z [m]
Decentralised MPC Control V1
Decentralised MPC Control V3

Figure 9f

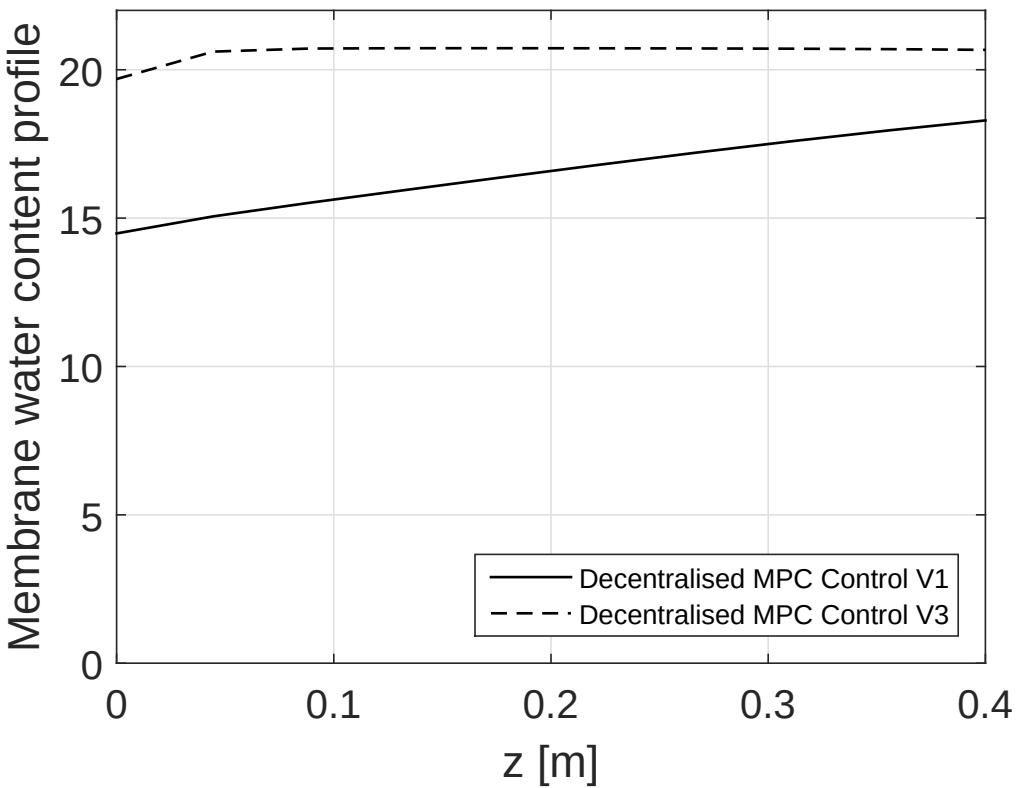
Membrane water content profile
20
15
10
5
0
0
0.1
0.2
0.3
0.4
z [m]
Decentralised MPC Control V1
Decentralised MPC Control V3

Editable Manuscript

Click here to download LaTeX Source Files: elsarticle-template.tex

References

Click here to download LaTeX Source Files: mybibfile.bib

Library

Click here to download LaTeX Source Files: elsarticle-num.bst

Library

Click here to download LaTeX Source Files: numcompress.sty

All files compressed

Click here to download LaTeX Source Files: Archive.zip